Multi-Aircraft Trajectory Optimization for Continuous Descent Arrivals

Arjun Puttabakula

TU Delft

Multi-Aircraft Trajectory Optimization for Continuous Descent Arrivals

by

Arjun Puttabakula

to obtain the degree of Master of Science in Aerospace Engineering
at the Delft University of Technology,
to be defended publicly on Tuesday January 26, 2017 at 14:00.

Specialization:	Air Transport and Operations	
Student number:	4419987	
Project duration:	April 1, 2016 – January 25, 2017	
Thesis committee:	Prof. dr. ir. Dries Visser,	TU Delft, Committee Chair
	Prof. dr. ir. Sander Hartjes,	TU Delft, Supervisor
	Prof. dr. ir. Mark Voskuijl,	TU Delft, External Committee Member

This thesis is confidential and cannot be made public until January 25, 2017.

TU Delft

PREFACE

The Master thesis at TU Delft has been one of the best experiences of my professional career. The past 10 months have been nothing short of a roller coaster ride. This thesis has been a tremendous learning experience with respect to expanding my knowledge base, time management, finding the right balance between professional and personal life. In short, I am not the same person I was when I first joined the Masters program.

This thesis would not be complete without the help of my supervisor dr. ir. Sander Hartjes. Sander has been very helpful and more importantly extremely patient with me during all the meetings and, is never short of ideas and reasoning. For me he will always be the perfect guide. I would also like to thank dr. ir. Dries Visser for being a constant presence in all of the progress meetings and pitching in useful ideas to improve my thesis.

Outside of work, my friends at Delft have been my biggest stress busters and were instrumental in keeping me sane. First and foremost I would like to thank ir. Srikar Yadala Venkata. Without a shadow of doubt he was a great support, always lending his ear for my thoughts, frustration and adding fuel to my ideas every single day in the past 10 months. Srikar was also my MATLAB teacher; everything I know in MATLAB today is because of him. I will always be greatful for his help and support. Many thanks to Mannat, Marco and Salil for all the game and talk nights, barbeques, drinks and making sure I don't talk about my thesis during these wonderful times we all spent together. Thanks to Shravan for clarifying my doubts all the way from Switzerland. Special thanks to Kashmira for all the motivation, working with me, lunch break talks and for all the things we did outside of work. I would like to thank Radesh for being a great supporter, always believing that I can do it. I would also like to extend my thanks to Apeksha, Ashwathi, Kiran and Prasobh for all the get togethers and dinners.

No words can truly express my gratitude for my girlfriend Sneha Srigiri. Many thanks to her for being so patient with me these past 2 years, constantly reminding me about what I am capable of and for just being there always when ever I needed you.

Finally, I would like to thank my parents and sister without whom none of this would have ever been possible. It is because of their immense sacrifice from the past 24 years that I stand here today. Nothing can ever replace what the three of you have done for me.

Arjun Puttabakula
Delft, January 10, 2017

SUMMARY

IT is a known fact that aircraft noise and fuel emissions are the most constraining factors for the growth of aviation. Continuous Descent Arrivals (CDAs) provide significant reductions in fuel consumption and noise footprint on the ground, by following idle thrust descent and eliminating low altitude leveling off. However, limitations such as unpredictability of the trajectory and separation management for CDAs prevent wide-spread implementation. The thesis focuses on overcoming some of these limitations. Optimal control theory is used to optimize the descent trajectory of the aircraft by using fuel and time as the performance index. The problem is formulated as a multi-phase optimal control and is solved by using a pseudospectral method. The theory is also the backbone of General Pseudospectral OPtimal Control Software (GPOPS). The main focus of the thesis is to enable multi-aircraft trajectory optimization for CDAs and ensure sufficient separation between all aircraft along the entire trajectory by implementing the separation algorithm. The possibility of using both distance based and the time based separation is explored in detail. It is demonstrated using Amsterdam Schiphol (AMS) airport's real-time inbound flight data that it is feasible to apply the separation algorithm to separate aircraft along the entire lateral path while still being able to perform CDAs during the peak and non-peak periods. All the limitations pertaining to the separation algorithm are analyzed and discussed in detail. By addressing some of these shortcomings, the simulation environment can be improved to bring it more close to a real-time scenario. Although a lot of other factors have to be considered for a practical wide-spread implementation, success of this method will result in the aircraft trajectory being more predictable to the ground controller, effectively addressing one of the major shortcomings of CDAs. On a more important note, the success of this method will also result in reduced noise footprint and fuel consumption by aircraft, benefiting both the environment and airlines.

Arjun Puttabakula
Delft, January 10, 2017

Contents

List of Figures

List of Tables

ACRONYMS

ADS-B	Automatic Dependent Surveillance-Broadcast
AIS	Aeronautical Information Service
AMS	Amsterdam Schiphol
AOC	Airline Operations Control Centre
ATC	Air Traffic Control
ATM	Air Traffic Management
BCOP	Boeing Climbout Program
CAS	Calibrated Air Speed
CDA	Continuous Descent Arrival
CDAs	Continuous Descent Arrivals
CTA	Controlled Time of Arrival
DBS	Distance Based Separation
ETA	Estimated Time of Arrival
FAA	Federal Aviation Administration
FAF	Final Approach Fix
FMS	Flight Management System
FPA	Flight Path Angle
GPOPS	General Pseudospectral OPtimal Control Software
HBVP	Hamiltonian Boundary Value Problem
IAF	Initial Approach Fix
IATA	International Air Transport Association
ICAO	International Civil Aviation Organization
KLM	Koninklijke Luchtvaart Maatschappij N.V.
LvNL	Luchtverkeersleiding Nederland
MTOW	Maximum Takeoff Weight
NAP	Noise Abatement Procedures
NATS	National Air Traffic Services
NextGen	Next Generation Air Transportation System
NLP	Non-linear Programming
PANS-OPS	Procedures for Air Navigation Services-aircraft OPerations
RNAV	Area Navigation

RTA	Required Time of Arrival
SESAR	Single European Sky ATM Research
SID	Standard Instrument Departure
SNOPT	Sparse Nonlinear OPTimizer
STAR	Standard Terminal Arrival Route
TBO	Trajectory Based Operations
TBS	Time Based Separation
TEMO	Time and Energy Managed Operations
TOD	Top-of-Descent
TRACON	Terminal Radar Approach Control
TSCDA	Time-based Spaced Continuous Descent Arrival
UPS	United Parcel Services
VNAV	Vertical Navigation
WVS	Wake Vortex Separation

1

INTRODUCTION

AIRCRAFT noise and emissions in the vicinity of airports, around the world, is a growing concern and is regarded as an industry-wide problem. It poses a significant threat to the environment and, has a profound impact on human health[9]. The aviation industry including the International Civil Aviation Organization (ICAO), International Air Transport Association (IATA) and Federal Aviation Administration (FAA) are increasingly focusing on reducing emissions and noise generated by aircraft. Projects such as Next Generation Air Transportation System (NextGen) by the United States and Single European Sky ATM Research (SESAR) by the European Union, aim to improve the efficiency of the air transportation system whilst reducing the environmental impacts of aviation. Worldwide, flights produced 781 million tonnes of carbon dioxide (CO_2) in 2015, which accounts for 12% of CO_2 emissions from all transport sources and 2% of all human-induced CO_2 emissions. IATA has taken numerous steps to tackle the issue of environmental impacts of aviation. In June 2009, IATA took a landmark decision to adopt a set of ambitious targets, endorsed by ICAO[20]. These ambitious targets include a cap on aviation CO_2 emissions from 2020, an average improvement in fuel efficiency of 1.5% annually from 2009 to 2020 and a 50% reduction in CO_2 by 2050, relative to the levels in 2005. In February 2016, ICAO approved a CO_2 efficiency standard for commercial aircraft. The standard to come into force from 2020, will ensure that CO_2 emissions from new aircraft meet a minimum baseline (defined as the maximum fuel burn per flight kilometre which must not be exceeded). From 2023, this will also apply to existing aircraft designs still in manufacture at that date[21].

Achieving the ambitious targets set by IATA and ICAO requires a combined effort from various organizations such as governments, airports and airlines. A third of airline's operating costs are spent on fuel and this is likely to increase as fuel prices increase further. This alone provides a major incentive for airlines to focus on fuel efficiency. As an alternative means to combat aircraft emissions and noise, Noise Abatement Procedures (NAP) have been studied since the late 1980's. They provide benefits of reducing noise footprints on the ground as well as fuel emissions depending on the procedure. It must be noted that certain NAP can also lead to increased emissions and derogate airport capacity at the cost of reduced noise around the airports. Procedures for Air Navigation Services-aircraft OPerations (PANS-OPS) provide guidelines for developing and implementing NAP in the vicinity of airports and along the departure path. Other NAP developed include tailored arrivals, Continuous Descent Arrivals (CDAs), nighttime preferential runway use, Noise Abatement Departure Procedures (NADP), low power/low drag approach profiles and reduced reverse thrust usage[22].

Continuous Descent Arrivals are one of the most beneficial and well recognized NAP. In a conventional approach procedure, the extended low level segments require a considerable amount of engine thrust, increasing fuel consumption and noise. CDA, as shown in figure 1.1,

is a new procedure in which the aircraft descends continuously under *idle thrust* and *clean configuration*, as much as possible, until the Final Approach Fix (FAF). Since CDAs are performed from cruise altitude and at idle thrust, it ensures that the aircraft altitude is as high as possible, for as long as possible, reducing both the noise generated on the ground and the fuel consumption. This procedure implemented at AMS airport for night-time operations demonstrated a reduction in fuel consumption by 25-40% and 30-55% smaller noise footprint during the last 45 *km* of the flight[43].

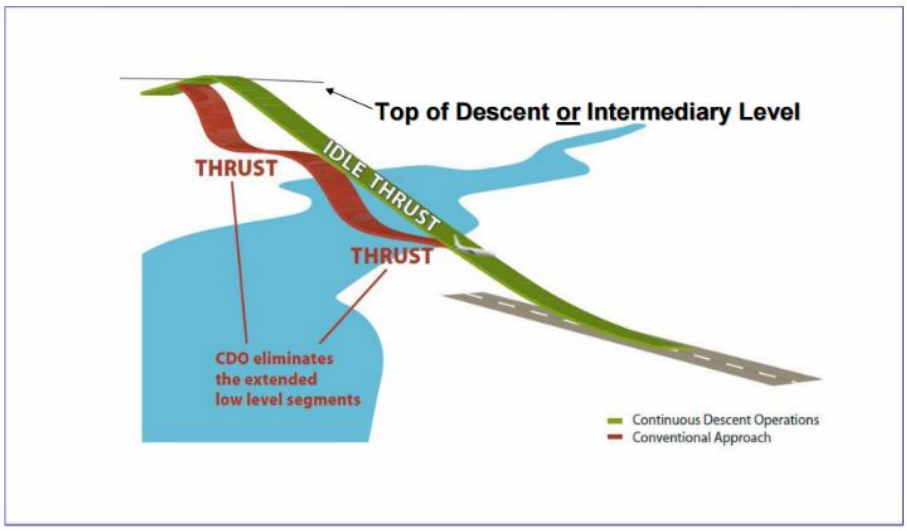

Figure 1.1: Continuous Descent Operations or Continuous Descent Arrivals.

Implementation of CDAs as a standard procedure is not possible for all arriving aircraft and the entire descent profile, the reasons for which will be discussed in section 2.1. Nevertheless, more airports are taking necessary steps to implement CDAs to the maximum extent possible and increase the percentage of CDA flights. For airlines and airports to be able to implement CDAs, ICAO's CDA implementation manual is under development. As an intermediate step, for Europe, CDA guidance material has been published by Eurocontrol - CDA Implementation Guidance Information[8].

The structure of this report is as follows: chapter 2 will emphasize on briefing the limitations of CDAs and the methodology used by different researchers in their simulated or practical implementation of CDAs. The research objective and goals of this thesis are then presented in detail. In chapter 3, a brief overview of optimal control theory and the various methods for solving them are outlined. Chapter 4 details the methodology that will be used to achieve the research objective. In chapter 5, the results obtained from the implementation of the methodology are presented and analysed in detail. In chapter 6, the conclusions of the research work along with possible limitations are explained and possible recommendations to improve on the current thesis are laid out.

2

State-of-Art

As discussed in chapter 1, CDAs provide significant reductions in noise footprints on the ground and fuel consumption. In spite of these benefits, widespread implementation of CDAs has not been possible. Section 2.1 gives a brief overview on the limitations of CDA. Section 2.2 and 2.3 aim to summarize the research being carried out to overcome these limitations. The research objectives of this thesis are then presented and detailed in section 2.4.

2.1 Limitations of CDA

Since CDAs are performed at idle thrust, the Air Traffic Control (ATC) has difficulty predicting the descent trajectory of the aircraft, as they vary not only based on wind, temperature and the speed of the aircraft, but also on airframe and engines[24]. Figure 2.1 depicts the unpredictability of the trajectory associated with CDAs due to different aircraft types and configurations. The trajectories were generated with the help of the Boeing Climbout Program (BCOP), under idle thrust and zero wind conditions for two aircraft types: a B737-700 and a B777-200. Start of the simulation is set at 35000 *ft*, 290 *kts* Calibrated Air Speed (CAS) and, ends at 11000 *ft* and 240 *kts* CAS[39]. It can be seen that the trajectories of the two aircraft are different. Also, a change in the Top-of-Descent (TOD) is observed for the B777-200 due to the change in deicing setting from low to high (red profile). The variations in the TOD are calculated by the aircraft itself and some of these parameters are unknown to the ATC, translating into differences between air and ground predicted speed and vertical profiles. Hence, the descent trajectories at idle thrust varies from one aircraft type to another and it's highly unpredictable nature is a major issue.

Furthermore, the trailing aircraft at a higher altitude is always faster than the leading aircraft at a lower altitude when both aircraft are performing a CDA. Since aircraft are not allowed to accelerate during the descent phase, this leads to shrinking of space between the leading and the trailing aircraft known as the *compression effect*[33]. Due to this compression effect and trajectory unpredictability, the ATC enforces a large separation of up to 4 minutes[43] between aircraft performing CDAs, affecting the runway throughput[32].

Other issues also hinder the widespread implementation of CDAs. Although PANS-OPS has guidelines for designing specific procedures, none exist for CDAs. This could be one of the reasons why there are multiple methodologies and implementations to apply CDAs by different researchers. Additionally, many airports around the world do not have the necessary ground equipment to easily asses the benefits of CDAs. One of the reasons for using this procedure only during low density traffic conditions can also be partially attributed to the additional pilot and ATC workload. CDA is a non-standard procedure and might involve additional constraints, making it difficult for the ATC to efficiently sequence flights. Other issues include economic

constraints, terrain and obstacles and lack of training[22].

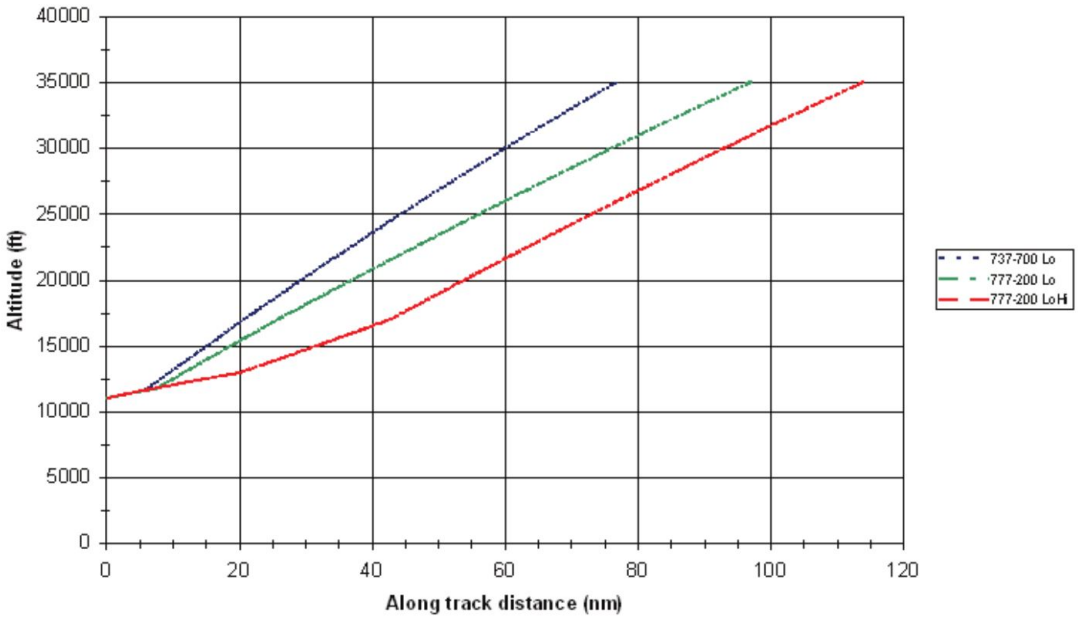

Figure 2.1: Trajectories of B737-700 and B777-200 - idle thrust, zero wind. Blue and green profile - low deicing, B737-700 and B777-200 . Red profile - B777-200, low deicing above 17,000 *ft* and high deicing below 17,000 *ft*. Reproduced from Tong *et al.* (2007)[39].

Developing a methodology to overcome trajectory unpredictability and interval management difficulties during CDAs are of paramount importance to realize it's widespread implementation, without affecting the runway throughput. A variety of approaches have been proposed by different researchers. Some of the procedures have been developed, trial runs carried out at specific airports to gather more data and understand to a greater extent the difficulties faced during the practical implementation of the approach.

2.2 State-of-Art

As stated in section 2.1, there are no specific guidelines for designing CDAs. Hence, the implementations by different researchers vary with respect to the start altitude and speed. This behavior is consistent across many research papers. As an example, in the research by Webben and Busink (2000)[43] and, Visser and Wijnen (2001)[40], the CDA simulations were performed from 7000 *ft* and 7000 *ft*/9000 *ft* respectively. In the research by Mulder *et al.* (2009)[28], CDAs were set to start at 9400 *ft* and end at 1000 *ft*, whereas for flight trials at Louisville International airport [5], CDAs started at 11000 *ft*. It is a well known fact that the aircraft noise has minimal impact on the ground when the aircraft is at or above 10000 *ft*, but performing CDAs from cruise altitude can provide significant benefits in fuel consumption and flight time. Some researchers perform simulations or flight trials from the cruise altitude. In reference[24,32,38,42], for example, CDAs were initiated from cruise altitude. Most simulations and flight trials for CDAs are designed to end when the aircraft intercepts the glideslope.

Another area of difference between these researches is the aircraft *type* used for simulations or flight trials. In the research by Webben and Busink[43], a B747-400 and a B737-300 were used. Mulder *et al.*[28] use an Airbus A330-200 for the simulations whereas in the research by Park and Clark[32], a B767 and a B737 aircraft were used. Flight trials for CDAs were conducted at Louisville International airport[5] with the help of UPS owned B757-200 and B767-300. The type and weight of the aircraft can have an impact on the fuel consumption and noise footprint on the ground.

A new generation aircraft with advanced aircraft engines produces less noise. A MD-11 and a B373NG were used for conducting flight trials for CDAs at AMS airport. Figure 2.2 clearly shows the noise contour difference, while performing a CDA, between the two aircraft.

(a) (b)

Figure 2.2: Noise contour during a CDA. (a) MD-11, (b) B737NG. Reproduced from Wat *et al.* (2006) [42].

The most viable and widely used option to implement CDAs by many researchers is by the *Flight Management System (FMS)* of the aircraft. This is because the next generation air traffic management (ATM) systems are still under development and a few years away from full fledged implementation. Data link and intent download will be a part of next generation systems and might overcome trajectory unpredictability issues. Since there is an urgent need to address environmental impacts of aviation, it is feasible to develop new procedures using existing system capabilities. Several implementations have focused on making use of the FMS capabilities to perform CDAs [5,24,28,42].

2.2.1 Continuous Descent Arrivals at Schiphol Airport

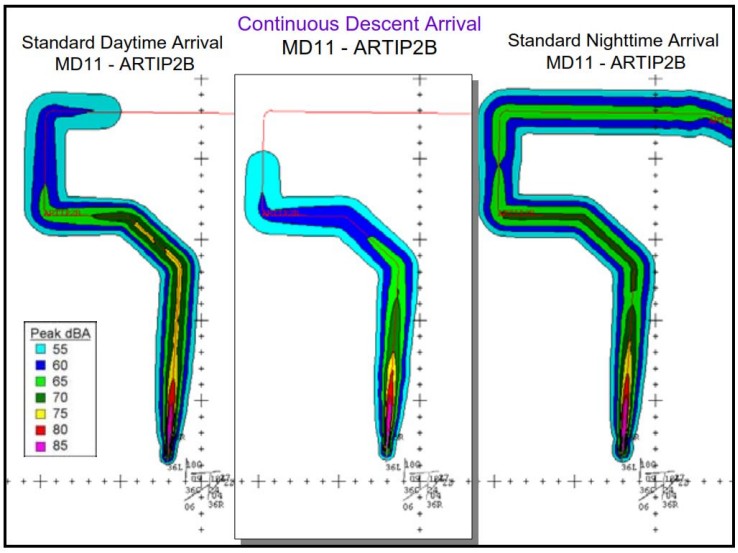

Figure 2.3: MD-11's noise contour analysis comparing a CDA and conventional approaches. Reproduced from Wat *et al.* (2006) [42].

The FMS based CDAs are currently in use at AMS airport[42]. The flight trials assessed the accuracy of the Estimated Time of Arrival (ETA) calculated by the FMS, coordination between Maastricht Upper Airspace Center (MUAC) and LvNL Flight Information Region (FIR) airspace, predictability of the trajectory, environmental impact and, workload of the ATC and the flight crew. The FMS would optimize the vertical profile within the specified operational constraints before reaching the TOD. The FMS calculated data was down linked via the Airline Operations Control Centre (AOC). Noise footprint analysis showed a 12 *dBA* and a 9 *dBA* improvement over the baseline procedure for a MD-11 and a B737 respectively. Fuel consumption was reduced by as much as 70% for a MD-11 and can be largely attributed to the elimination of level segment at 3000 *ft*. Figure 2.3 gives a pictorial representation of the reduced noise footprint of a MD-11 aircraft performing a CDA, when compared to conventional approaches.

2.2.2 Continuous Descent Arrivals at Louisville International Airport

Similarly, CDAs were designed and developed for night time operations at Louisville International airport by Clarke *et al.* (2004)[5]. Vertical trajectory planning, including operational constraints such as altitude and airspeeds at waypoints, was implemented using the FMS Vertical Navigation (VNAV) function. Data obtained from flight trials showed noise reductions between 3.5 *dBA* and 6.5 *dBA* for the two aircraft used in the trials: a B757 and a B767. This reduction is significant since a 3 *dBA* difference represents a 50% reduction in acoustic energy, noticeable to the human ear. Also, the data obtained from the aircraft during the CDA procedure is compared with data obtained during the conventional approach based on track distance, altitude profile, fan speed, flap extension, speed break usage (to help stay on the proposed vertical profile), flight time and fuel consumption giving the researcher a good idea about how each of these parameters vary between the two procedures. Following the success of these flight trials, UPS has obtained the license to perform at least two CDAs for night-time operation.

2.2.3 Time-based Spaced Continuous Descent Arrival (TSCDA)

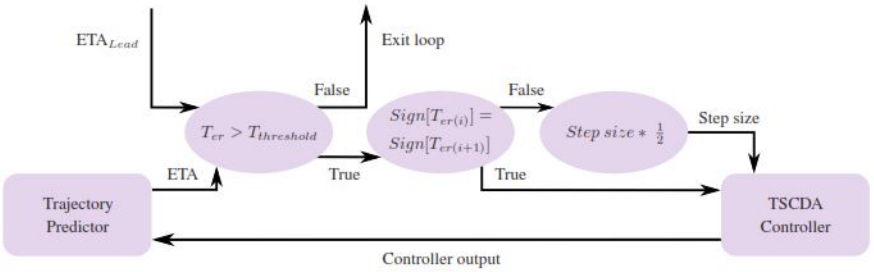

Figure 2.4: Main control loop of TSCDA. Reproduced from Mulder *et al.* (2009)[28].

The Time-based Spaced Continuous Descent Arrival (TSCDA) concept, proposed by Mulder *et al.* (2009), to calculate precise inter arrival spacing is based on the accurate computation of the ETA by the FMS[28]. This ETA is then sent to the trailing aircraft using an Automatic Dependent Surveillance-Broadcast (ADS-B) transponder. The three controllers ensure that the inter arrival spacing (T_{space}) between the aircraft in the arrival stream is equal to $120s$ at the runway threshold. The algorithm works by either controlling thrust by the Thrust Controller (TC), next flap configuration speed by the Flap/Gear Scheduler (FGS) or the speed of the aircraft by the Speed Constraint Deviation controller (SCD), such that the spacing error T_{er} (difference of the ETA and the Required Time of Arrival (RTA)) between the leading and the trailing aircraft at the runway threshold is less than or equal to $1.5s$. All the three controllers use spacing error T_{er} as their *input*. Figure 2.4 shows the main loop used by the TSCDA controller. Simulations were performed with the three controllers taking into account the varying wind condition, aircraft

weight, arrival stream set up and position in arrival stream. Based on the analysis and results, the SCD showed the least deviation for varying conditions and also performed the best.

2.2.4 3D Path Concept

A different approach was proposed by Tong *et al.* (2007) known as the *3D Path Concept*[39]. The idea here is to make use of a constant Flight Path Angle (FPA) and different *fixed* lateral path options known as *lateral stretching*, to cope with high traffic during descent. The concept of using lateral stretching to allow the ATC to manage separation is exploited by the *3D PAM concept*[16]. Aircraft descent with a constant FPA makes the trajectory more predictable for the ATC. Even though some thrust (less than that necessary for level flight) is required to maintain a constant FPA, Tong *et al.* argue that with proper design the projected reductions in noise, fuel burn and flight time are still reasonable. Implementation of this concept into the FMS is also detailed, but as stated by the authors, "to be able to fully utilize the 3D path concept, a ground based automation tool is required that should be able to predict a descent trajectory on the ground that emulates the descent profile constructed by the airborne FMS with sufficient accuracy for all the aircraft models in the current fleet". In spite of these limitations, the 3D Path Concept was applied to develop CDAs for dual-runway operations at Houston Intercontinental (IAH) as detailed by Tong *et al.* (2006)[38]. Figure 2.5 represents the additional path options (3D PAM concept) used by the ATC to enable separation of aircraft in both en-route airspace and the Terminal Radar Approach Control (TRACON) area. Additionally, the authors propose a small level segment to facilitate re-planning before entering the TRACON area and, making use of different glideslope intercept altitudes to provide the required vertical separation on parallel runways.

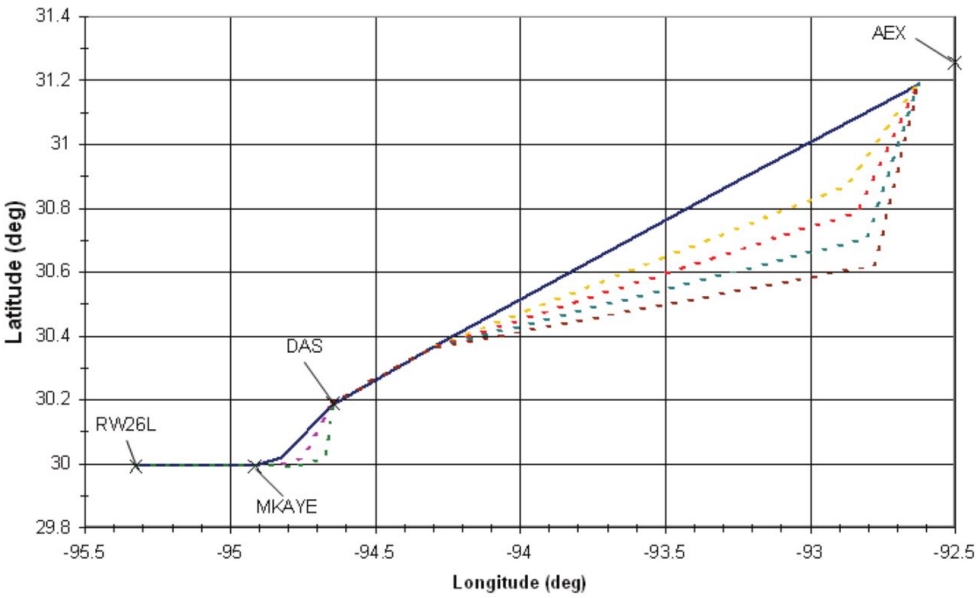

Figure 2.5: Design of lateral path using the 3D PAM concept for CDA operations at IAH. Reproduced from Tong *et al.* (2006)[38].

2.2.5 Time and Energy Managed Operations (TEMO)

de Jong *et al.* (2014) developed a new algorithm for CDA named Time and Energy Managed Operations (TEMO) and uses the notion of energy modulation to control the aircraft to a given point in space and time[7]. A Controlled Time of Arrival (CTA) is issued to an aircraft flying a TEMO at the Initial Approach Fix (IAF) and at the runway threshold to which it has to adhere. If the error between the aircraft time and energy at the current position and, the planned state at

that position exceeds a certain value ($\pm 4s$), TEMO calculates a new trajectory by incorporating *strategic re-planning*. TEMO commands an increase in the CAS or it might loose altitude quickly to compensate for the *late* time error and, use speed breaks to reduce the CAS to solve an *early* time error. An enhanced version of TEMO was illustrated by Prats *et al.* (2014)[34]. The new algorithm takes into account the effect of wind fields and non-standard atmospheric conditions.

2.2.6 Trajectory Based Operations (TBO)

The air traffic management system is slowly transitioning towards Trajectory Based Operations (TBO). Aircraft would be capable of 4D trajectory (4DT) execution with lateral and vertical navigation performance bounds, including the RTA guidance functionality. Klooster *et al.* (2008) point out that TBO might be a possible solution for the lack of predictability inherent in flying CDAs[24]. Flight trials with Scandinavian Airlines, in 2001, whose aircraft were equipped with these advanced functionalities demonstrated that the time-of-arrival control accuracy at waypoints was less than $7s$ with a mean of 4.8 s and, the control accuracy was bounded to 21 s with a mean of 12.7 s at the runway threshold. Further flight trials conducted in 2007 with an updated FMS software demonstrated a 38.5% improvement from a mean of 12.7 s to 7.8 s, with a standard deviation of 4.1 s. The periodic downlink of 4DT was used to examine the effect of wind and other parameters on the stability of the trajectory. The paper highlights the requirement of accurate forecast of winds to precisely know the 4D trajectory of the aircraft. This is because considerable variability in the trajectory can occur depending on the wind conditions as shown in figure 2.6 for a B737-600 aircraft. The authors also propose making use of a *constant gradient* in high density traffic conditions, to constrain the altitude profile of an aircraft in case accurate wind forecasts are not available.

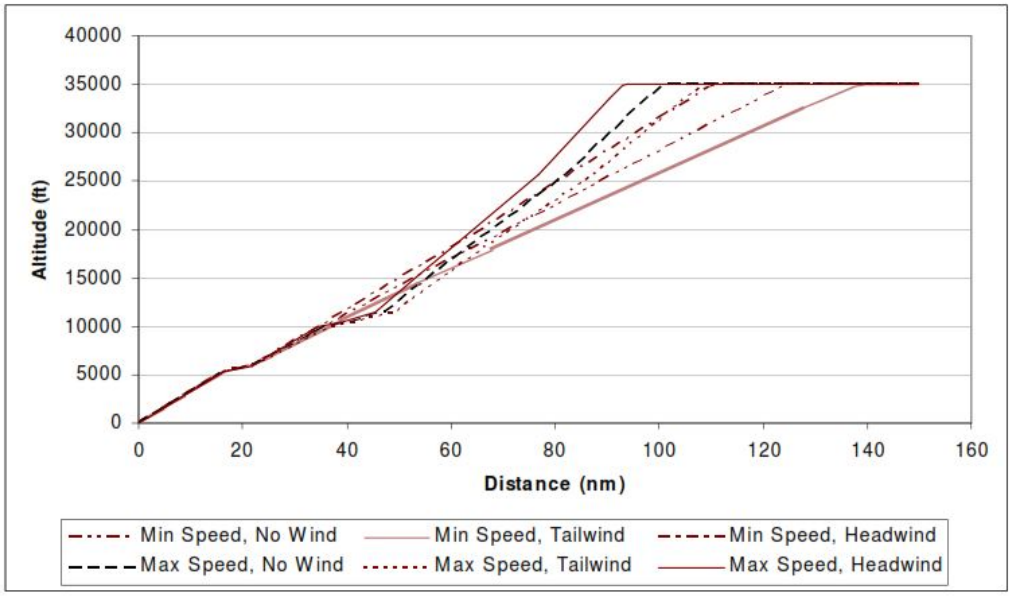

Figure 2.6: Trajectory variability due to varying wind conditions for a B737-600 during idle thrust CDA. Reproduced from Klooster *et al.* (2008)[24].

2.2.7 The Role of ATC in Noise Abatement Procedures

The Air Traffic Control plays a significant role in minimizing noise around airports. The ATC generally has the power to intervene, while the aircraft is performing NAP, if it compromises on safety. Depending on the conditions, the ATC gives clearance to the flight crew to perform a CDA, but the ATC generally underestimates the remaining track distance from the runway threshold and, might issue early descent clearances. Hence, it becomes difficult for pilots to

estimate the optimum descent rate, affecting the propensity of the flight crew to perform and achieve a successful CDA. An 'early' descent clearance can result in the aircraft flying lower than desired and, force the aircraft to make a level segment to compensate for it. If ATC can improve their range estimates, more aircraft can successfully follow NAP[23].

2.3 Previous Research Based on Optimal Control Theory

Another approach often used by researchers for optimizing the vertical trajectories of aircraft is based on the *optimal control theory*. Implementation of optimal control theory for optimizing trajectories of aircraft and helicopters has already been done before by researchers[18,30–32,40]. Trajectory optimization techniques facilitate coupling of vertical and horizontal routings. Several trajectory optimization techniques have been proposed by previous researchers. Most researchers use energy as the independent variable instead of time, resulting in simplified aircraft dynamic equations. Also, important operational requirements instrumental for practical implementation such as flap extension schedules, speed limits, etc., are often not taken into account.

2.3.1 Optimization of Noise Abatement Arrival Trajectories

Visser and Wijnen (2001) performed an optimization study for noise abatement arrival procedures at AMS airport[40]. The authors assert that the *EZopt* package used is capable of dealing with a large number of path constraints resulting from operational and safety requirements. The approach used is unique since it combines a noise model, a geographic information system and a dynamic trajectory optimization algorithm. The number of people within the exposed community that are expected to be awakened due to a single night-time noise intrusion is used as the primary performance index. Based on the collocation method, the EZopt package transforms the optimal control problem into a Non-linear Programming (NLP) problem, by discretizing the trajectory dynamics. The noise abatement arrival procedure was initiated from 7000 *ft* and, then from 9000 *ft* in a separate scenario. Results indicated that a higher initial altitude does provide benefits with respect to awakenings and fuel consumption, as shown in figure 2.7. At initial altitudes higher than 10000 *ft*, lateral stretching will be required to absorb the excess energy.

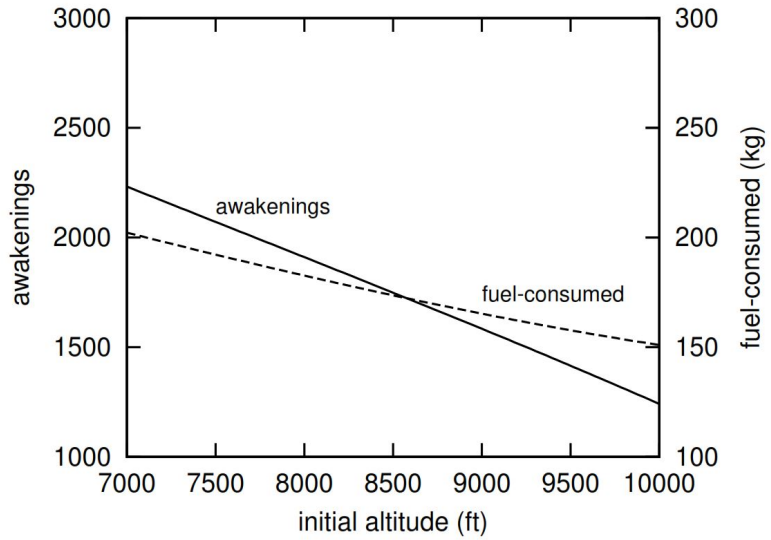

Figure 2.7: Comparison of optimal performance for various initial altitudes. Reproduced from Visser and Wijnen (2001)[40].

2.3.2 Vertical Trajectory Optimization for CDA

Park and Clarke (2015)[32] use multi-phase optimal control based on the pseudospectral method to optimize vertical trajectories for CDAs. The authors analyze the performance bounds of CDAs with *flight time and fuel consumption* as the two performance indices. All the phases are formulated based on operational constraints such as FAA speed limit regulations, flap/gear schedules, etc., as shown in figure 2.8. The initial along track distance is free. Hence, it is possible to calculate both the optimal TOD and CDA trajectory. Optimal trajectories were calculated for two aircraft types: a B737-500 and a B767-400. GPOPS[36] coupled with a Sparse Nonlinear OPTimizer (SNOPT)[14] is used to obtain optimal trajectories. Area Navigation (RNAV) CDA profiles were constructed by parameterizing the control inputs and operating constraints. A comparison is made between the optimal trajectories calculated by GPOPS and trajectories calculated by the RNAV function of the FMS. For the minimum time case, the trajectories of both were found to be the same, while a small performance degradation was observed for the minimum fuel case. These results indicate that a practical implementation of this approach is possible.

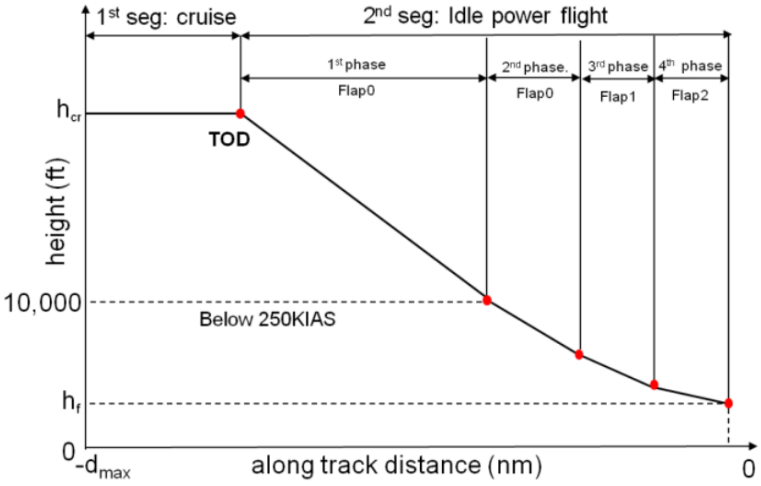

Figure 2.8: Multi-phase formulation for vertical trajectory optimization. Reproduced from Park and Clark (2015)[32].

2.4 Research Objectives

Most of the previous research (based on optimal control theory) for CDAs has been focused on trajectory optimization of a single aircraft. Not much research has been carried out to apply this technique for optimization of multiple trajectories and to simulate a flight sequence for arrival in which all aircraft fly following CDAs, whilst satisfying the operational requirements.

The concept proposed by Park and Clarke (2015)[32] can be extended further to determine the optimal trajectories of all trailing aircraft also performing CDAs. Such an implementation can only be feasible if sufficient separation can be maintained between aircraft performing CDAs and ensuring that the system capacity is not compromised in the process. This thesis focuses on exploring and studying such a scenario. Hence, the main research objective would be to,

Optimize, with respect to time, the descent trajectories of all aircraft performing Continuous Descent Arrivals, by using optimal control theory, whilst maintaining the required separation and system capacity.

The focus will be on answering the following questions which would eventually give a clear answer to the main research question,

- What is the most suitable method that can be used for aircraft arrival trajectory optimization?
  - What are the different trajectory optimization techniques that can be used?
  - What are the advantages and disadvantages of each technique?
  - Why is the chosen technique most suitable for CDA trajectory optimization?
- Is the methodology developed for simulating CDAs applicable in medium to high density traffic conditions?
- What kind of separation methodology is being applied to ensure sufficient separation between the aircraft?
  - What kind of separation methodology will yield the best results?
  - Will time based separation, distance based separation or a combination of both be more suitable?
- Is the designed methodology generic - for implementation at any airport?

2.4.1 Research Goals

To answer the above research objective effectively, it's important to formulate a set of research goals:

- **ATC regulations:** A good understanding of the ATC rules and regulations will provide an idea about how close the simulations are to the actual operating environment. It also helps to incorporate some of these regulations as constraints during the mathematical formulation of the problem. It is of particular interest to understand how the ATC manages separation in medium to high traffic conditions when aircraft are following a conventional approach. Some of these techniques might also be applied in the simulation to maintain separation while aircraft are performing CDAs.
- **Evaluation of numerical methods for trajectory optimization:** This involves understanding the basics of optimal control theory and all the various methods available for solving optimal control problems. Having some insight about the differences between each of these methods would be helpful in choosing the best method for a specific problem.
- **Developing the mathematical formulation**: Once we have sufficient understanding about optimal control and the various trajectory optimization techniques, the next step would be to formulate the problem mathematically for the specific problem. The formulation should be developed being aware of the control to be minimized.
- **Finding a suitable software solution:** A number of software solutions are available that use different forms of optimal control and, they might be applicable only for solving a specific type of problem(s). It is important to find a suitable software that uses the theory chosen by the researcher as it's backbone and run the simulation with the results obtained from the software solution.
- **Design the separation algorithm and optimize aircraft on CDAs**: The chosen software solution is used to optimize the trajectory of aircraft performing CDAs and the results of

single-aircraft optimized trajectory is used as constraints for optimizing the trajectory of the trailing aircraft. The required separation between them is ensured by the separation algorithm, both in en-route airspace and the TRACON area. Mulder *et al.* (2009) [28] proposal for time-based separation can be investigated further to use in combination with optimal control theory for simulation. The 3D PAM concept [16] introduces the idea of using pre-designed lateral paths to facilitate the use of CDAs in high density traffic conditions. Hence, time-based separation [28], distance based separation [16,39] or a combination of both might be useful and will be analyzed in detail. The use of a constant FPA [39], for making the trajectory more predictable, can be implemented as constraint in the trajectory optimization formulation. The energy state of an aircraft during descent should also be considered. To release the excess energy, the optimal trajectories might be stretched laterally, violating operational requirements and, generate more noise. In this regard, the research by de Jong *et al.* (2014) [7], where the notion of energy modulation is used to control the aircraft can be useful. Park and Clark (2015) [32] show that the optimal trajectories generated using optimal control theory are almost similar to the ones generated by the FMS. Implementation of CDAs using the FMS is particularly useful for reasons already stated in section 2.2.

- **Simulation using real-time data**: At some point during the simulation, 24-hour arrival data from AMS airport will be of particular interest. The data is useful in the sense that it gives an idea of the aircraft type mix, which are sequenced for landing at AMS airport and can be used to perform simulations. If relevant operational constraints are also included in the simulation, it gives an idea about how close the results are to a real-time operating environment. It might also be feasible to consider optimization of aircraft performing CDAs on different lateral paths. In such a case, the algorithm should also be capable of maintaining the required separation when aircraft are merging at a common waypoint.

3

Optimal Control Theory

Optimal control theory is the theoretical basis of this thesis. There have been numerous advancements in this field and its applications in various engineering domains have resulted in optimal control being considered as a new field of engineering itself. Optimal control theory aims to find the controls that perturb a system from a fixed initial condition to a free or fixed final condition, whilst minimizing the total value of a cost functional, which itself is a function of the system controls and states. In other words, from among all admissible control functions, optimal control theory finds that one, which minimizes the performance criterion subject to the dynamic constraints and all the initial and terminal boundary conditions that may be specified. Optimal control problems may be interpreted as an extension of the nonlinear programming problem to an infinite number of variables[2].

Due to the vast field of optimal control and several advancements made in the last two decades, there are a large variety of methods and types of optimal control. Hence, it is important to focus the research to a specific area in optimal control to meet the research objectives. It is of interest to use optimal control theory to find the optimal trajectory the aircraft can follow while reducing the performance index, which can either be a function of time, fuel or noise. In this regard, the research by Betts (1998) gives a good overview of optimal control theory with respect to trajectory optimization and detailing the various numerical methods available for solving optimal control problems of this type[2]. Optimal control problems are generally non-linear and therefore do not have analytic solutions. As a result, it is necessary to employ numerical methods to solve them.

3.1 Multi-phase Continuous Bolza Problem

Before reviewing in detail about the numerical methods available to solve optimal control problems, it is essential to discuss the type of optimal control problem formulation used for this thesis. The so-called *continuous Bolza problem* is used. In a continuous Bolza problem, the objective function 'J' consists of both the Mayer form and the problem of Lagrange. The problem is also formulated as a combination of phases. The end states of the previous phase are linked to the initial states of the next phase with a phase link constraint. Specifically for trajectory optimization problems, the concept of phases becomes important. Phases are introduced in an optimal control problem formulation when different differential equations are to be used for different stages of the problem or they can also be introduced to impose specific constraints. Hence, the trajectory optimization problem is formulated as a *multi-phase* continuous Bolza problem[2].

3.1.1 General Formulation of Multi-phase Continuous Bolza Problem

In it's most general form, the control $u(t) \in \mathbb{R}^m$ is to be determined to minimize the performance index or Bolza cost functional[32],

$$J = \sum_{p=1}^{N} \left[\phi^{(p)}\left(x^{(p)}(t_0), t_0, x^{(p)}(t_f), t_f\right) + \int_{t_0}^{t_f^{(p)}} L^{(p)}\left(x^{(p)}, u^{(p)}, t\right) dt \right] \tag{3.1}$$

where $x(t) \in \mathbb{R}^n$ is the state, t_0 is the intial time, t_f is the final time, which can be either free or fixed and, $p = [1, 2, ..., N]$ represents the number of phases. In equation 3.1, ϕ represents the Mayer cost or terminal cost and L represents Lagrangian of the p^{th} phase respectively.

The cost functional is subjected to the following constraints,

- Dynamic constraints
$$\dot{x}^{(p)} = f^{(p)}\left(x^{(p)}, u^{(p)}, t\right) \tag{3.2}$$
- Event constraint at each phase
$$\phi_{min} \leq \phi^{(p)}\left(x^{(p)}(t_0), t_0, x^{(p)}(t_f), t_f\right) \leq \phi_{max} \tag{3.3}$$
- Algebraic path constraints
$$g_{min} \leq g^{(p)}\left(x^{(p)}, u^{(p)}, t\right) \leq g_{max} \tag{3.4}$$
- Phase link constraint
$$P^{(s)}\left(x^{(p-1)}, t_f^{(p-1)}, x^{(p)}, t_0^{(p)}\right) = 0 \tag{3.5}$$

3.2 Methods for Solving Optimal Control Problems

As discussed earlier, to find solutions to optimal control problems, various methods exist. Figure 3.1 provides a general classification of methods for solving optimal control problems.

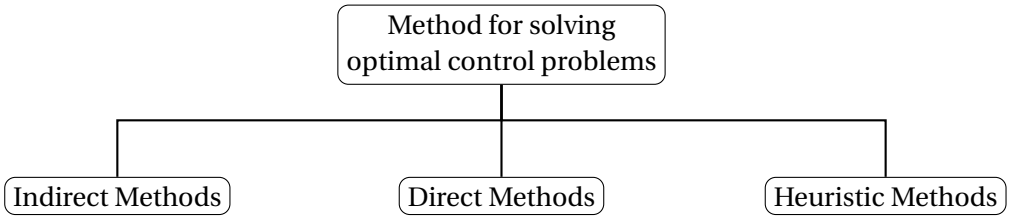

Figure 3.1: General classification of methods for solving optimal control problems.

3.2.1 Indirect Methods

In earlier days, *indirect methods* were the most preferred techniques. The method is based on the maximum principle or *calculus of variations*[13]. The calculus of variations is used to calculate the first-order optimality conditions (derived using an augmented Hamiltonian $\mathscr{H}$). The Hamiltonian system, along with the boundary conditions, transversality conditions and complementary slackness conditions is called a *Hamiltonian Boundary Value Problem (HBVP)*[25]. The solutions to a HBVP are called *extremals* and are determined numerically. Each of the computed extremals is then examined to see if it is a local minimum, maximum, or a saddle

point. Of the locally optimizing solutions, the particular extremal with the lowest cost is chosen [35]. The most popular indirect methods for solving optimal control problems are shown in figure 3.2.

In general, indirect methods are fairly simple and produce highly accurate results when solutions converge. One major advantage is that it is possible to find the global optimum using indirect methods [18]. However, indirect methods suffer from sensitivity issues with respect to the initial guess. If the initial guess is poor, it can result in "wild" trajectories. This is because the extremal solution is often sensitive to small changes in the unspecified boundary conditions [2]. Also, due to computational limits of computers, the method was applied only to specific cases in which the problem contains few path constraints and phases and, the underlying dynamics of the problems were very clearly defined. Indirect methods also require derivation of first order optimality conditions for every new problem and, for a complex problem the process can become tedious and impossible in certain cases. One of the very well known software solutions that is based on the indirect method of optimal control is BNDSCO [15].

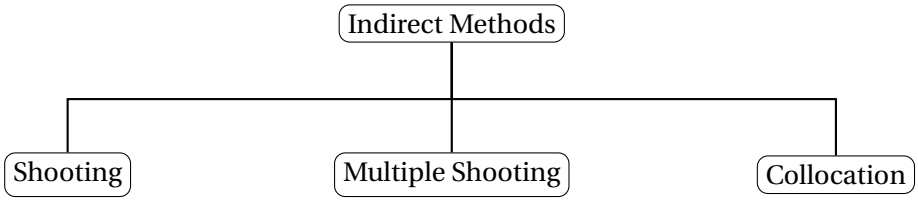

Figure 3.2: Classification of indirect methods for solving optimal control problems.

3.2.2 Direct Methods

In the past two decades, the *direct method* for solving the optimal control problem has risen to prominence. In direct methods, the state and/or controls of the optimal control problem are discretized and transformed into a *NLP* problem. In other words, the solution to the optimal control problem using direct methods is found by transcribing an infinite-dimensional optimization problem to a finite-dimensional optimization NLP problem. The various direct methods for solving optimal control problems are shown in figure 3.3. The direct local collocation method leads to a large but *sparse* NLP (i.e., the NLP has tens of thousands of variables and equal number of constraints, but many of the derivatives in the constraint Jacobian are zero). Hence, it is possible to solve them using well known NLP solvers such as Sparse Nonlinear OPTimizer (SNOPT) [14].

Moving on, in a *pseudospectral (PS) method* the state is approximated using a *global* polynomial

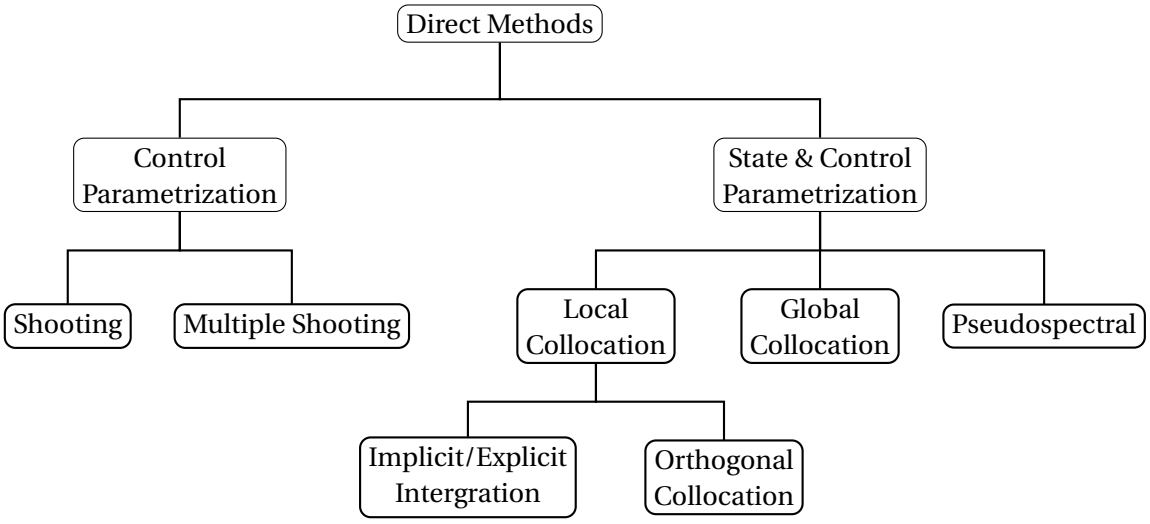

Figure 3.3: Classification of direct methods for solving optimal control problems.

and collocation is performed at chosen points. In a local orthogonal collocation method, the basic polynomial is fixed while meshes are varied. In a PS method, it is vice-versa i.e., the meshes are fixed while the basic polynomial is varied. As stated by Garg *et al.* (2010), "pseudospectral methods are a class of direct collocation where the optimal control problem is transcribed to a Non-linear Programming by parameterizing the state and control using global polynomials and collocating the differential-algebraic equations using nodes obtained from a Gaussian quadrature"[11]. The three most commonly used sets of collocation points are Legendre-Gauss (LG), Legendre-Gauss-Radau (LGR) and Legendre-Gauss-Lobatto (LGL). For trajectory optimization problems, the LG and LGR methods show best convergence. Also, it can be shown that for problems having either a fixed initial or fixed final time, the Radau method generally shows better convergence behavior[19]. Some of the well known software solutions that implement direct methods are SOCS[3], DIRCOL[41], OTIS[17], GESOP/ASTOS[12] and DITAN[1], to name a few.

3.2.3 Heuristic Methods - Genetic Algorithms

All of the above mentioned techniques come under a general classification known as *gradient methods*. They are also famously known as local methods because after convergence, a *local* minima/maxima is obtained. Although gradient methods are only capable of finding a local minimum, with careful formulation (if the problem is convex), the solution can be a global minimum. Also, with the help of gradient methods, it is possible to include a lot of parameters and the run-time is in the order of few seconds. On the other hand, heuristic methods are *global* methods. They are incredibly simple to apply and, do not require a detailed understanding of the system. Unlike gradient menthods, the run time for heuristic methods can extend to days. The various heuristic methods for solving optimal control problems are shown in figure 3.4.

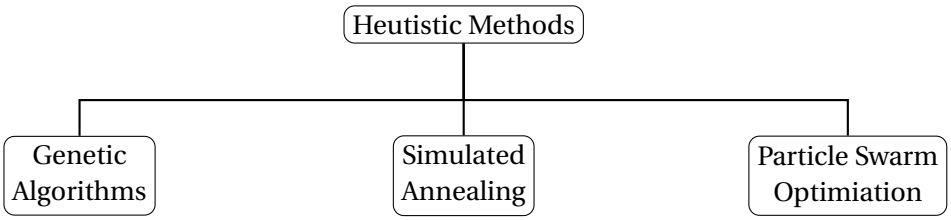

Figure 3.4: Classification of heuristic methods for solving optimal control problems.

Genetic Algorithms (GAs), one of the well known heuristic methods, is an adaptive search algorithm based on the evolutionary ideas of natural selection and genetics. An initial population of possible solutions to a problem is chosen. Based on "survival of the fittest" concept by Charles Darwin, the solution consists of genes that are more fit and likely to survive the next generation. These genes are then recombined (i.e., they are mutated) via a crossover mechanism, which results in future generations of populations. Continuing generationally, those genes with the highest fitness survive to the later generations[35]. These methods are most suitable for introducing randomness (for unknown variables) into a problem consisting of discrete variables, but trajectory optimization problems are *continuous* and do not fall in this category[2]. In spite of this, GAs have been used in some applications (for example, interplanetary trajectory optimization[4]), but by no means as widespread as gradient methods.

3.3 Experimental Set-Up

3.3.1 General Pseudospectral Optimal Control Software (GPOPS)

For a highly complex problem, involving a large number of states and control variables, direct collocation methods are the most suitable. With present day computational capabilities of

computers, NLP solvers can be used to obtain a solution to the optimal control problem and are specially designed to converge with poor initial guesses. The application of PS methods has been on the rise since the past couple of years[37]. Due to its independently reproducible superior performance when compared to other techniques, PS methods have found application in ascent guidance[26], lunar landing, launch vehicle trajectory optimization, etc.

Rao *et al.* (2010) developed the General Pseudospectral OPtimal Control Software in MATLAB[36] for solving continuous optimal control problems using *hp*-adaptive Gaussian quadrature collocation and sparse non-linear programming[6]. GPOPS also employs both the Legendre-Gauss and Legendre-Gauss-Radau methods. As stated by Rao *et al.* (2010)[36], "GPOPS employs *hp*-adaptive Gaussian quadrature collocation method, which is a hybrid between a *p* method and a *h* method in that both the number of mesh intervals and the degree of the approximating polynomial within each mesh interval can be varied, in order to achieve a specified accuracy in the numerical approximation of the solution to the continuous-time optimal control problem. Hence, it is possible to take advantage of the exponential convergence of a global Gaussian quadrature method in regions where the solution is smooth and introduce mesh points only near potential discontinuities or in regions where the solution changes rapidly." SNOPT, which employs a sparse sequential quadratic programming (SQP) algorithm, is a software designed to solve large-scale nonlinear optimization problems[14]. It is especially effective for non-linear problems with functions and gradients that are expensive to evaluate. GPOPS has SNOPT integrated into it as a NLP solver.

On the flip side, in cases where the functions are continuous but the derivatives are discontinuous, GPOPS may struggle because SNOPT is not being provided with accurate approximations to the derivative functions. Additionally, constraint qualification conditions may not be satisfied on fine meshes if the problem has high-index path constraints. For such cases, unique NLP Lagrange multipliers may not exist or Lagrange multipliers may become unbounded.

This particular thesis makes use of GPOPS as its backbone as far as the programming and simulation is concerned. The idea is to build the simulations around the optimal trajectories calculated by the GPOPS software. The performance bounds of a single-aircraft optimal trajectory is used as constraints to optimize the trajectory of the trailing aircraft, while ensuring required separation with the help of a separation algorithm. It is also important to note that to the maximum extent possible, operational constraints will be implemented in the simulation environment.

4

METHODOLOGY

IN this chapter, the methodology incorporated to facilitate multi-aircraft trajectory optimization is described in detail. In section 4.1, basic information about operations at AMS airport and types of CDAs are discussed. It is followed by point-mass model (section 4.2) and the lateral path design used in this thesis (section 4.3). Finally, the aircraft separation algorithm to facilitate multi-aircraft trajectory optimization are discussed in section 4.4.1 and 4.4.3.

4.1 OPERATIONS AT AMSTERDAM SCHIPHOL AIRPORT

The simulation design used in this research is based on the geography of Amsterdam Schiphol airport. AMS airport is the main international airport of the Netherlands. It is also KLM's main hub airport with approximately 70% of KLM passengers traveling through AMS airport being transfer passengers. AMS airport has 5 main operating runways. The 6^{th} runway is used for general aviation. Although the number of runways are high compared to other airports, their relative position and orientation and, noise restrictions limit simultaneous operations on a combination of runways.

Two types of CDA techniques exist, namely *tactical CDAs* and *advanced CDAs*. Their definitions are vastly dependent on the lateral path design. In a tactical CDA, the lateral path followed by the aircraft is defined through specific instructions provided by the ATC to the flight crew, otherwise known as *vectoring*. In an advanced CDA, the lateral path of the aircraft is pre-defined and is based on the Standard Terminal Arrival Route (STAR). Both the techniques have advantages and disadvantages which are as follows.

- **Runway throughput** - When following a pre-defined lateral route in an advanced CDA technique, a buffer needs to be created for aircraft with different speeds. This buffer leads to reduced runway throughput. In a tactical CDA technique, with aircraft following different routes, the need for this buffer is eliminated.
- **Workload** - Tactical CDAs can increase the workload of both the ATC and the flight crew. The ATC has to provide relevant instructions to all aircraft and manage both lateral and vertical separation, while the flight crew has to implement the instructions and possibly make changes to the flight settings, adjust descent rate depending on the remaining track distance, etc.
- **Noise affected area** - Due to the fixed lateral paths in an advanced CDA technique, the noise is concentrated on to a limited area and noise levels can be quite high, although it must be noted here that pre-defined lateral routes are designed to fly over less populated

areas and follow AMS airport's strict noise regulations. In a tactical CDA technique, noise is dispersed over a wide area due to varying aircraft tracks.

AMS airport's daily operations are based on the concept of alternating peak periods (periods in which either the arriving or departing traffic is predominant). To facilitate this, during the peak periods, three runways are in use. During the arrivals peak, for example, two of the runways are used for arrivals while the third runway is dedicated for departures only. The combination of runways used throughout the day and year varies based on strict noise regulations. In AMS airport, the noise preferential runway system is in place. The highest preference is given to operations on runways that lead to less noise nuisance in the densely populated areas, also taking into account the prevailing weather and visibility conditions. Runways 18R and 06 have the highest preference in the arrivals peak runway preference order. In general, preference 1 (arrivals - 06, 36R; departures - 36L), 2 (arrivals - 18R, 18C; departures - 24) and 3 (arrivals - 18R, 18C; departures - 18L) account for 90% of arrival peaks during the year[27].

Continuous Descent Arrivals are currently in use at AMS airport for night-time operations between 23:00 to 06:00[42]. This procedure was developed by the LvNL and is based on the advanced CDA technique. The CDA procedure simulated in this thesis is also based on the advanced CDA technique.

Figure 4.1: Standard lateral routings in FIR. Reproduced from Wat *et al.* (2006)[42].

Since runways 18R and 06 have the highest preference and in reference with figure 4.1, the lateral paths chosen for simulations are also based on these runways. In section 4.3, the lateral path

design to ensure that the aircraft lands on the runway 18R (as an example) is detailed and is in congruence with the lateral path design shown in figure 4.1. The information pertaining to all the lateral paths shown in this figure are published in Aeronautical Information Service (AIS) Netherlands. The AIS charts contain all the relevant information about the AMS airport such as the runways, the STAR charts, the SID charts, waypoint coordinates, etc.

4.2 Point-mass Model

An integrated intermediate point-mass model for aircraft performance modeling is used in GPOPS. The model consists of five states (x, y, z, V, χ) and three controls (γ, μ, η). It is based on the assumptions that there is no wind factor present, the Earth is flat and non-rotating and the flight is coordinated. All the calculations are performed in standard atmospheric conditions. The point-mass model's equations of motion can then be defined as,

$$\dot{x} = V \,.\, \cos\gamma \,.\, \sin\chi \tag{4.1}$$

$$\dot{y} = V \,.\, \cos\gamma \,.\, \cos\chi \tag{4.2}$$

$$\dot{z} = V \,.\, \sin\gamma \tag{4.3}$$

$$\dot{V} = g\,\frac{\frac{(T-D)\,V}{W} - \dot{z}}{V} \tag{4.4}$$

$$\dot{\chi} = g\,\frac{\tan\mu}{V} \tag{4.5}$$

where (x, y) are aircraft mass center coordinates in the Earth north-east-down inertial frame, z is the altitude in meters, V is the velocity in ms^{-1}, γ is the FPA in radians, χ is the heading angle in radians, μ is the bank angle in radians, T is the thrust in Newtons, D is the drag in Newtons, W is the weight of the aircraft in kg and g is the acceleration due to gravity in ms^{-2}.

In it's current form, GPOPS can optimize both the lateral and the vertical trajectory of the aircraft simultaneously for a CDA. In order to design the lateral path, all the waypoint coordinates and heading angles of the lateral path are given as inputs to GPOPS and it requires a multi-phase formulation of the problem. Each phase in the problem differs only with respect to the waypoint conditions (x_i, y_i, χ_i and x_f, y_f, χ_f). It must be noted that there is 1) no change in the dynamics of the aircraft between each phase, 2) no additional constraints or 3) no change in vertical parameters to justify the use of multiple phases. The use of multiple phases also meant that computation times are longer, when compared with a single phase problem.

Since CDAs in this thesis are based on the advanced CDA technique, the lateral path of the aircraft is fixed at all times. Hence, it is necessary to only perform vertical trajectory optimization in GPOPS. The parameters affecting the lateral path of the aircraft are eliminated i.e., aircraft mass center coordinates (x, y) , heading angle χ and bank angle μ. The point-mass model now has only three states (z, V, d) and two controls (γ, η) and can be defined as,

$$\dot{z} = V \,.\, \sin\gamma \tag{4.6}$$

$$\dot{V} = g\,\frac{\frac{(T-D)\,V}{W} - \dot{z}}{V} \tag{4.7}$$

$$\dot{d} = V \,.\, \cos\gamma \tag{4.8}$$

The aircraft mass center coordinates (x, y) are converted to ground track distance d. The bank angle μ is also a function of the constant turn radius R_i and the velocity V of the aircraft at that point on the turn. The bank angle μ can then be defined as,

$$\mu = \tan^{-1}\left(\frac{V^2}{g\,R_i}\right) \tag{4.9}$$

where R_i is the turn radius in m, V is the velocity of the aircraft in ms^{-1} and g is the acceleration due to gravity in ms^{-2}.

With the point-mass model defined by equations 4.6-4.8 , the vertical trajectory of the aircraft is optimized for a specified ground track distance d.

4.3 Lateral Path Design

The lateral path design is done to geometrically determine the effective distance d_e to be travelled by the aircraft along a pre-defined lateral path. This effective distance d_e is then given as input to GPOPS. The aircraft vertical trajectory is then optimized for this specified effective distance d_e. The geometric calculations required to compute the effective distance d_e are illustrated in figure 4.2.

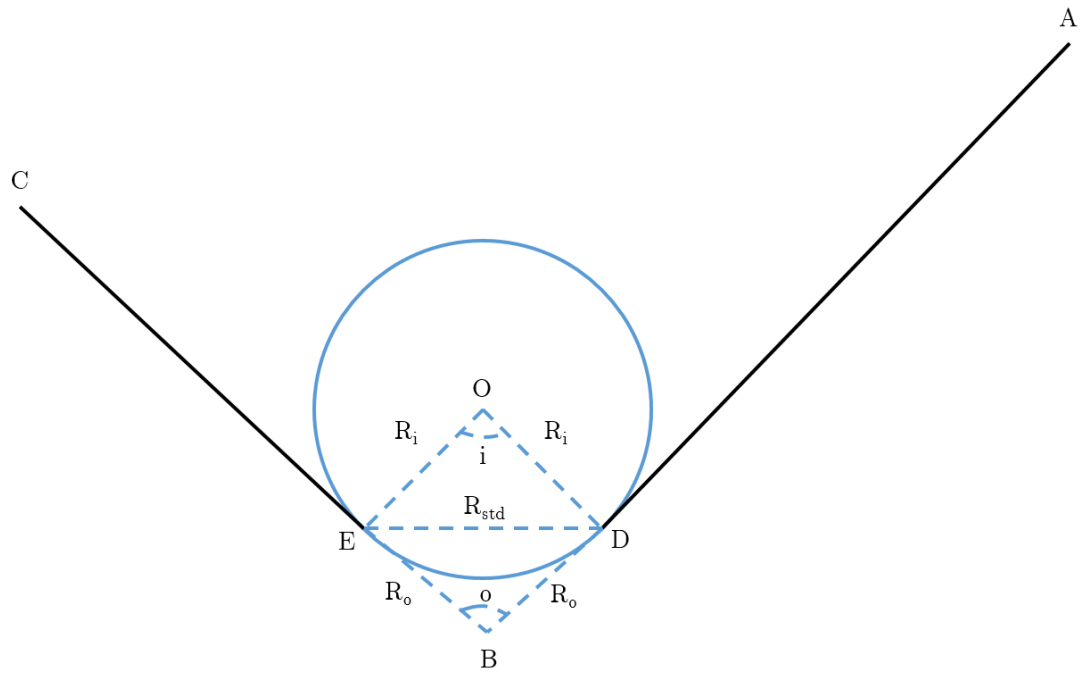

Figure 4.2: Geometric illustration for the lateral path design.

It is assumed that the aircraft travels from the waypoint A to the waypoint C, passing through the waypoint B. The coordinates of the waypoints A, B and C are known and hence the distance d_{AB} and d_{BC} can be computed. A circle with radius R_i is drawn such that $\overline{AB}$ and $\overline{BC}$ are tangents to the circle. The intersection of the tangents results in the included angle $\angle o$ between the three waypoints. Since the turns also have to be modelled in the lateral path, the total distance travelled along the turns i.e., sum of d_{AD}, d_{DE} (arc DE) and d_{EC}, is less than the distance travelled between the waypoints i.e., sum of d_{AB} and d_{BC}. Based on the geometry, the effective distance d_e is given by the equation,

$$d_e = d_{AD} + d_{DE} + d_{EC} \tag{4.10}$$

where d_{AD} is the distance between the waypoint A and the point D, d_{DE} is the arc length between the point D and E and d_{EC} is the distance between the point E and the waypoint C. With the help of the geometry, the distances d_{AD}, d_{DE} and d_{EC} are computed as follows.

Since BDOE forms a quadrilateral, the included angle $\angle i$ of the sector OED is,

$$\angle i = 360^\circ - \angle ODB - \angle OEB - \angle o \tag{4.11}$$
$$\angle i = 180^\circ - \angle o \tag{4.12}$$

Consider the isosceles triangle ΔODE. The length of the chord R_{std} can be computed using the law of cosines and is given by,

$${R_{std}}^2 = {R_i}^2 + {R_i}^2 - 2 \,.\, R_i \,.\, R_i \,.\, \cos(\angle i) \tag{4.13}$$

Consider the isosceles triangle ΔBDE. With R_{std} computed from equation 4.13, applying the law of cosines again and rearranging the terms, R_o can be computed.

$${R_o}^2 = \frac{{R_{std}}^2}{2\,[\,1 - \cos(\angle o)\,]} \tag{4.14}$$

Hence,

$$d_{AD} = d_{AB} - R_o \tag{4.15}$$
$$d_{EC} = d_{BC} - R_o \tag{4.16}$$

Arc length,

$$d_{DE} = 2\pi R_i \left(\frac{\angle i}{360^\circ}\right) \tag{4.17}$$

Hence, the effective distance d_e can be calculated with all the variables known.

Having computed all the required distances (to calculate the effective distance d_e) and knowing the $(x,\ y)$ coordinates of all the waypoints (A, B and C), the $(x,\ y)$ coordinates of all the other points in the geometry can be computed i.e., point D $(x_D,\ y_D)$, E $(x_E,\ y_E)$ and center of circle O $(x_C,\ y_C)$. Similar computations are extended for lateral paths comprising of multiple turns and also for the design of different lateral paths used in this thesis.

4.3.1 Post Processing

The trajectory is optimized in GPOPS for the specified effective distance d_e and the initial and final conditions. In post processing, using the heading angle χ, the effective distance d_e is converted to $(x,\ y)$ coordinates to geometrically illustrate the lateral path followed by the aircraft. The following formulas are used to convert the effective distance d_e to $(x,\ y)$ coordinates,

For straight paths,

$$x_i = x + d_i \,.\, \cos\chi \tag{4.18}$$
$$y_i = y + d_i \,.\, \sin\chi \tag{4.19}$$

where $(x_i,\ y_i)$ are the coordinates of the current point to be computed, $(x,\ y)$ are the initial coordinates of the straight path, d_i is the distance traveled by the aircraft between $(x_i,\ y_i)$ and $(x,\ y)$ and, χ is the heading angle of the straight path.

For the first straight path, the $(x,\ y)$ coordinates are always the initial point of the lateral path i.e., $(x_1,\ y_1)$. For all the subsequent straight paths the $(x,\ y)$ coordinates will be equal to the terminal coordinates of the turn preceding it. In the geometry shown in figure 4.2, the $(x,\ y)$ coordinates of point A in the straight path $\overline{AD}$ is $(x_1,\ y_1)$. To calculate the $(x_i,\ y_i)$ coordinates of the straight path $\overline{EC}$, the $(x,\ y)$ coordinates in equation 4.18 and 4.19 refer to the coordinates of point E $(x_E,\ y_E)$ i.e., the terminal coordinates of the turn represented by the arc DE.

For the constant radius turns, the parametric representation of a circle is used.

$$x_i = x_C + R_i \,.\, \cos(\Delta\theta) \tag{4.20}$$

$$y_i = y_C + R_i \,.\, \sin(\Delta\theta) \tag{4.21}$$

where $(x_C,\ y_C)$ are the coordinates of the center of the circle and R_i is the turn radius. Also,

$$\Delta\theta = \frac{\Delta d}{R_i} \tag{4.22}$$

where Δd refers to the distance travelled by the aircraft from the start of the turn to the current point for which the $(x,\ y)$ coordinates are being computed i.e., $(x_i,\ y_i)$.

The lateral paths designed for this thesis along with the resulting effective distances d_e and geometric illustrations are presented in chapter 5.

4.4 Aircraft Separation Algorithm

In order to facilitate multi-aircraft trajectory optimization for CDAs, sufficient separation must be ensured between aircraft at every point in time. In the current day-to-day operations, aircraft are separated by the ATC based on distance, also known as Distance Based Separation (DBS). The aircraft separation algorithm designed in this thesis is also based on DBS. As per standard ATC practices, all aircraft have to be separated by at least 5 *NM* in en-route airspace and by at least 3 *NM* in the TRACON area, unless otherwise specified.

4.4.1 Distance Based Separation - Same Lateral Path

The first aircraft, hereinafter referred to as the leading aircraft AC1, entering the sector is optimized for a specified effective distance d_e. When the second aircraft, hereinafter referred to as the trailing aircraft AC2, enters the sector, the leading aircraft AC1 trajectory is *fixed* and independent of the trajectory of the trailing aircraft AC2. The trailing aircraft AC2 always takes maximum penalty to ensure separation along the entire trajectory with the leading aircraft AC1.

The distance d_1 and the time t_1 of the leading aircraft AC1 are matrices containing discretized values, such that each element in the distance matrix d_1 corresponds to the distance travelled by the aircraft in the corresponding time t_1. Once GPOPS completes the optimization of the leading aircraft AC1, the distance d_1 and the time t_1 are linearly extrapolated and a 10^{th} degree polynomial is generated which best fits the function,

$$d_1 = f(t_1) \tag{4.23}$$

The trailing aircraft AC2 distance d_2 and time t_2 matrices have their own discretized values. The 10^{th} degree polynomial represented by equation 4.23 is evaluated for the trailing aircraft AC2 optimization time t_2 but with an initially assumed time lag Δt.

$$d_{1_2} = f(t_2 + \Delta t) \tag{4.24}$$

This results in a new distance matrix d_{1_2}, which represents the distance the leading aircraft AC1 would have travelled for the discretized time steps $t_2 + \Delta t$ of the trailing aircraft AC2. The initially assumed time lag Δt is introduced to ensure that the leading aircraft AC1 has a head start along the pre-defined lateral path. In other words, the trailing aircraft AC2 is assumed to enter the sector after a time Δt.

Due to the introduction of the initially assumed time lag Δt, the polynomial generated (without linear extrapolation) will have to be evaluated outside the range of time t_1 of the leading aircraft

AC1. The behavior of a high degree polynomial is highly unpredictable when evaluated outside the range for which it was initially generated. Linear extrapolation of the distance d_1 and time t_1 of the leading aircraft AC1 ensures that when the polynomial (equation 4.23) is evaluated for the time $t_2 + \Delta t$, it still falls within the range for which the high degree polynomial was generated. Subtracting the distance d_{1_2} of the leading aircraft AC1 with the distance d_2 of the trailing aircraft AC2 will result in the separation distance d_{sep} between the two aircraft along the entire trajectory.

$$d_{sep} = d_{1_2} - d_2 \tag{4.25}$$

4.4.2 Distance Based Separation - Different Lateral Path

In an effort to make the simulation environment as close as possible to a real-time traffic situation at an airport, trajectory optimization of aircraft arriving from two different lateral paths but landing on the same runway is considered. For the trajectory optimization of aircraft which are on two different lateral paths, it is important to consider the spatial positions of both aircraft. Unlike in section 4.4.1, where only the distance travelled by the aircraft along the same trajectory is used to calculate the separation distance d_{sep}, when the two aircraft are arriving from two different lateral paths, their spatial positions are used to calculate the separation distance.

Consider two aircraft arriving from two different lateral paths but landing on the same runway - 18R; the leading aircraft AC1 arriving from the East to the runway 18R and the trailing aircraft AC2 arriving from the West to the runway 18R. Since the lateral paths are pre-defined, it is possible to calculate the spatial positions of both aircraft based on the distance covered by them along their respective lateral paths. Consider the leading aircraft AC1. Based on the leading aircraft AC1 distance matrix d_{1_2},

For straight paths,

$$x_1 = x + d_{1_2} \,.\cos\chi \tag{4.26}$$
$$y_1 = y + d_{1_2} \,.\sin\chi \tag{4.27}$$

where $(x_1,\ y_1)$ are the coordinates of the current point to be computed, $(x,\ y)$ are the initial coordinates of the straight path, d_{1_2} is the distance covered by the leading aircraft AC1 between $(x,\ y)$ and $(x_1,\ y_1)$ and, χ is the heading angle of the straight path.

For the constant radius turns,

$$x_1 = x_C + R_1 \,.\cos(\Delta\theta_1) \tag{4.28}$$
$$y_1 = y_C + R_1 \,.\sin(\Delta\theta_1) \tag{4.29}$$

where $(x_C,\ y_C)$ are the coordinates of the center of the circle and R_1 is the turn radius. Also,

$$\Delta\theta_1 = \frac{\Delta d_1}{R_1} = \frac{d_{1_2} - d_t}{R_1} \tag{4.30}$$

where Δd_1 refers to the distance traveled by the aircraft from the start of the turn to the current point for which the $(x,\ y)$ coordinates are being computed i.e., $(x_i,\ y_i)$.

The distance matrix d_{1_2} is derived from equation 4.24. This implies that the position of the leading aircraft AC1 along the trajectory is already being considered with the initially assumed time lag Δt.

Thus, $(x_1,\ y_1)$ gives the spatial position of the leading aircraft AC1 at all the corresponding discrete time $t_2 + \Delta t$ of the trailing aircraft AC2. In a similar fashion, the spatial position of the

trailing aircraft AC2 i.e., $(x_2,\ y_2)$ can be computed at all the corresponding discrete time t_2 of the trailing aircraft. Having calculated the spatial positions of both aircraft, the separation distance d_{sep} between them can be computed as follows,

$$d_{sep} = \sqrt{(x_1 - x_2)^2 + (y_1 - y_2)^2} \tag{4.31}$$

4.4.3 Time Based Separation - Same Lateral Path

Although this thesis focuses on DBS, as a part of the next generation Air Traffic Management (ATM) systems, NextGen and SESAR are actively working on TBS between aircraft. In the presence of a strong headwind, the ground speed of the aircraft is reduced. This results in more separation between the aircraft, reducing the runway throughput. TBS aims to maintain the runway throughput at airports even in light and strong headwind conditions. Due to the headwinds, the wake vortex generated by the aircraft is dispersed faster. This, in turn, facilitates reduced separation between aircraft without compromising on safety. Hence, the delays and cancellations caused due to DBS coupled with headwinds at airports is avoided. TBS is already in use at the London Heathrow (LHR) airport and replaces previous ICAO distance-based wake separation standards[29]. The technology is developed by National Air Traffic Services (NATS), which is the main air navigation service provider in the United Kingdom.

The leading aircraft AC1 entering the sector is optimized for a specified effective distance d_e. When the trailing aircraft AC2 enters the sector, the leading aircraft AC1 trajectory is *fixed* and independent of the trajectory of the trailing aircraft AC2. The trailing aircraft AC2 always takes maximum penalty to ensure separation along the entire trajectory with the leading aircraft AC1.

The distance d_1 and the time t_1 of the leading aircraft AC1 are matrices containing discretized values, such that each element in the distance matrix d_1 corresponds to the distance travelled by the aircraft in the corresponding time t_1. Once GPOPS completes the optimization of the leading aircraft AC1, the distance d_1 and the time t_1 are linearly extrapolated and a 10^{th} degree polynomial is generated which best fits the function,

$$t_1 = f(d_1) \tag{4.32}$$

The trailing aircraft AC2 distance d_2 and time t_2 matrices have their own discretized values. The 10^{th} degree polynomial represented by equation 4.32 is evaluated for the trailing aircraft AC2 optimization distance d_2.

$$t_{1_2} = f(d_2) \tag{4.33}$$

This results in a new time matrix t_{1_2}, which represents the flight time of the leading aircraft for the discretized distance d_2 of the trailing aircraft AC2. Subtracting the time $t_{1_2} + \Delta t$ of the leading aircraft with the time t_2 of the trailing aircraft will result in the separation time t_{sep} between the two aircraft along the entire trajectory.

$$t_{sep} = t_{1_2} + \Delta t - t_2 \tag{4.34}$$

where Δt is the initially assumed time lag. The initially assumed time lag Δt is introduced to ensure that the leading aircraft AC1 has a head start along the pre-defined lateral path. In other words, the trailing aircraft AC2 is assumed to enter the sector after a time Δt.

5

RESULTS

IN this chapter, results of up to 11 scenarios are presented. An effort has been made to include unique scenarios to best explain the behaviour of the trailing aircraft due to the implementation of the aircraft separation algorithm. To validate the aircraft separation algorithm, results obtained from simulation of AMS airport's real-time inbound flight data are presented and discussed in detail. Additionally, a comparison of computation time is made between selected scenarios to highlight the impact of the aircraft separation algorithm on GPOPS.

5.1 SINGLE-AIRCRAFT TRAJECTORY OPTIMIZATION

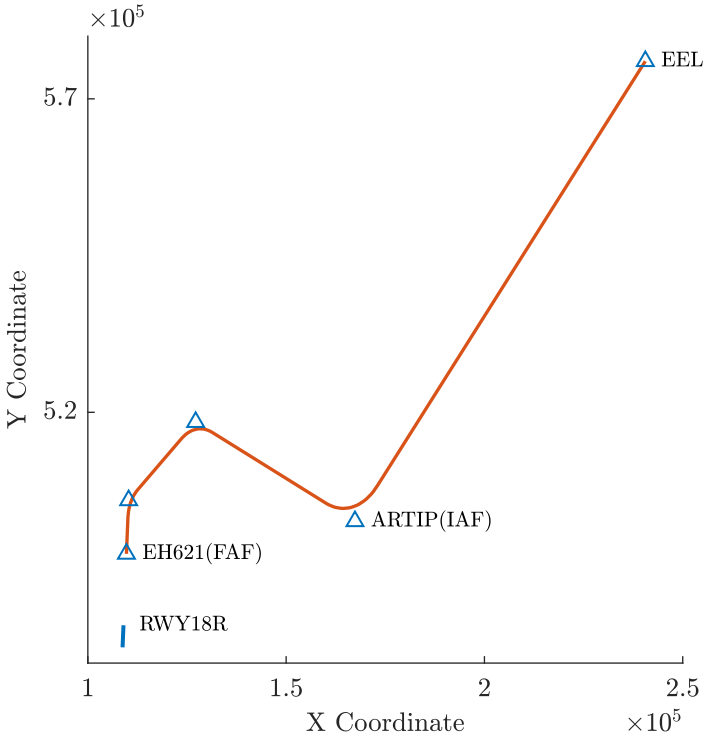

Figure 5.1: Lateral path followed by the aircraft arriving from the East of the runway 18R. All units in *m*.

The aircraft performance model (section 4.2) coupled with the lateral path design (section 4.3) are implemented in GPOPS to optimize the trajectory of a B744 aircraft. Single-aircraft trajectory optimization is performed on a specific lateral path such that it's arrival runway is 18R. The designed lateral path is shown in figure 5.1 and results in an effective distance d_e of 173.45 *km*.

All the intermediary way points and the runway 18R are marked in this figure for reference. The turn radius R_i is chosen such that the computed bank angle at each turn is greater than 5° and less than 25°. The trajectory followed by the aircraft along with the altitude profile can also be reproduced on Google Earth for better representation and is shown in figure 5.2.

Figure 5.2: Google Earth representation of lateral path followed by the aircraft arriving from the East of the runway 18R.

Since the performance characteristics of all aircraft vary when they are on the glideslope path, the optimization is designed to end when the aircraft reaches the FAF (EH621) at an altitude of 2000 *ft*. It is assumed that the aircraft intercepts the glideslope at the FAF. From this point (FAF) on until the runway threshold, the aircraft is on the 3° glideslope path, which is not part of the optimization. The various parameters used for single-aircraft optimization in GPOPS are shown in table 5.1.

Table 5.1: Optimization parameters for single-aircraft optimization.

PARAMETER	VALUE
Cost function	Time
Initial Altitude (z_i)	28000 *ft*
Initial Speed (V_i)	317.2 *kts* CAS (0.8 *Mach*)
Final Altitude (z_f)	2000 *ft*
Final Speed (V_f)	170 *kts* CAS
Arrival Runway	18R
Lateral Path Waypoints	EEL - ARTIP - NARIX - EH608 - EH621
Effective Distance (d_e)	173.45 *km*
No. of Phases	2
Aircraft Types	B733, B738, B744 & MD11

In order to implement the mandatory FAA constraint , which restricts the CAS of the aircraft to a maximum of 250 *kts* at or below 10000 *ft* [10], the problem is formulated in two phases. The first phase is designed to end when the aircraft reaches an altitude of 10000 *ft*. At this altitude, GPOPS ensures that the aircraft CAS is at or below 250 *kts*.

The following constraints are also implemented in addition to the FAA constraint, altitude and speed limits shown in table 5.1.

- The aircraft is only allowed to decelerate during the CDA procedure and is implemented as a path constraint in all phases. All units in ms^{-2}.

$$-2 \leq \dot{V}_{CAS} \leq 0 \tag{5.1}$$

- The aircraft is not allowed to climb during the CDA procedure and is implemented as a path constraint in all phases. All units in ms^{-1}.

$$-100 \leq \dot{z} \leq 0 \tag{5.2}$$

- The Flight Path Angle γ during the optimization are defined by the following limits in each phase,

$$-5^\circ \leq \gamma^{(1)} \leq 0^\circ \tag{5.3}$$
$$-5^\circ \leq \gamma^{(2)} \leq -2^\circ \tag{5.4}$$

  Equation 5.4 ensures that below an altitude of 10000 *ft*, the aircraft does not make a level segment.

The altitude, CAS, thrust and FPA profiles of the aircraft are shown in figure 5.3. It can be seen from figure 5.3a that the aircraft makes a level segment at 28000 *ft* before its descent. This level segment is not specifically modeled in GPOPS. The optimizer is free to choose the most appropriate TOD based on the remaining track distance. The aircraft again makes a level segment at 10000 *ft* before the start of phase 2. This is acceptable since at 10000 *ft* or above, the effect of aircraft noise on the ground is negligible. It must also be noted from figure 5.3c that the normalized thrust of the aircraft when it is at 10000 *ft* is zero; hence there is no effect of engine noise due to this level segment. In phase 2, the aircraft descends from 10000 *ft* to the final altitude of 2000 *ft* without making any level segment. Therefore, the FPA γ condition specified by equation 5.4 is satisfied and is in congruence with the FPA profile shown in figure 5.3d.

The trajectory is optimized with respect to time. Hence, GPOPS ensures that the aircraft CAS is as high as possible, for as long as possible, to reach the destination faster. It can be observed from figure 5.3b that the optimizer utilizes the aircraft level segment at 10000 *ft* to dissipate kinetic energy and reduce the CAS to 250 *kts*. This is to ensure that the mandatory FAA constraint is satisfied. It must also be noted from figure 5.3c that the aircraft utilizes thrust only to maintain level flight at 28000 *ft*. From the TOD until the aircraft reaches 2000 *ft*, the thrust is at idle.

Due to the varying performance characterstics of different aircraft types, the flight time of each aircraft is different. Table 5.2 shows the flight time of each aircraft type during single-aircraft trajectory optimization.

Table 5.2: Comparison of flight time during single-aircraft trajectory optimization.

AIRCRAFT TYPE	FLIGHT TIME (*s*)
B733	938
B738	983
MD11	983
B744	1000

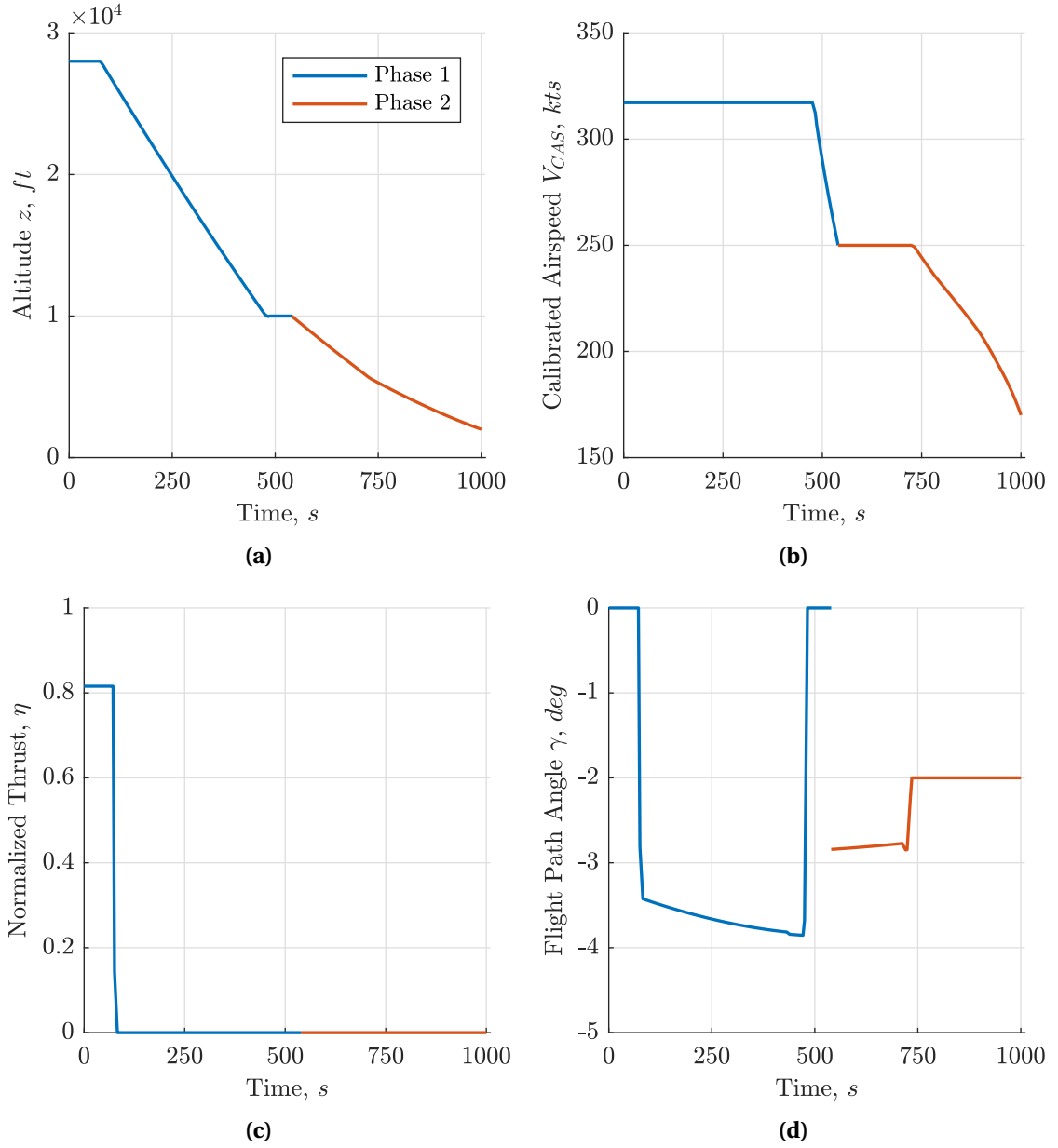

Figure 5.3: Single-aircraft trajectory optimization for aircraft type - B744. (a) Altitude profile, (b) Calibrated Air Speed profile, (c) Thrust profile, (d) Flight Path Angle profile.

It is important to note here that the trajectories obtained are as close as possible to a CDA and do not follow the actual definition of a CDA procedure. To simulate a true CDA procedure, the constraints will have to be fomulated in such a way that the optimizer is forced to enforce a CDA, which is usually undesireable.

5.2 Dual-Aircraft Trajectory Optimization - Same Lateral Path

Having obtained satisfactory results from the single-aircraft trajectory optimization (section 5.1), the distance based separation algorithm discussed in section 4.4.1 is applied and a second aircraft - the trailing aircraft AC2 is introduced in the sector. The trailing aircraft AC2 trajectory is optimized on the same lateral path as shown in figure 5.1 and also for the same initial and final conditions given in table 5.1. The separation constraint, represented by equation 4.25, is

implemented as a path constraint in both phases and is defined as,

$$d_{WVS} \leq d_{sep}^{(1)} \leq d_{max} \tag{5.5}$$

$$d_{WVS} \leq d_{sep}^{(2)} \leq d_{max} \tag{5.6}$$

where d_{WVS} is the minimum required Wake Vortex Separation (WVS) between the leading aircraft AC1 and trailing aircraft AC2 and, d_{max} is the maximum distance the aircraft can travel. All units in *m*.

The minimum required WVS between the two aircraft is dependent on their weight category[29] and the ICAO Distance Based Separation standards. The WVS implemented in this thesis between the available aircraft types is shown in table 5.3. The four available aircraft are categorized into different weight categories based on the Maximum Takeoff Weight (MTOW) of the aircraft.

Table 5.3: Wake vortex separation minima in *NM*.

		Trailing		
Leading	**Weight Category**	**Small**	**Medium**	**Heavy**
	Small	3	3	3
	Medium	4	3	3
	Heavy	6	5	4

Table 5.4: Aircraft Weight Category in *kg*.

Weight Category (kg)	**Aircraft Type**
Small (> 17000 & ≤ 40000)	
Medium (> 40000 & ≤ 136000)	B733 & B738
Heavy (≥ 136000)	B744 & MD11

Due to unavailability of data for various aircraft models in the upper medium weight category, the lower medium and upper medium weight categories have been clubbed into a single weight category (medium) as shown in table 5.4. Also, in cases where the separation distance d_{sep} between the aircraft does not depend on WVS alone (for example, medium - heavy combination), a minimum of 3 *NM* is assumed.

The trailing aircraft AC2 is always assumed to enter the sector after an initially assumed time lag Δt. For all the scenarios, unless otherwise specified, the values of the initially assumed time lag Δt are based on table 5.5. It is important to note here that the values in table 5.5 are not based on any standard, but a set of values which are assumed for the purpose of simulation. In a real-time operating environment these values will vary.

Table 5.5: Initial assumed time lag Δt in *s*.

		Trailing		
Leading	**Weight Category**	**Small**	**Medium**	**Heavy**
	Small	35	35	35
	Medium	65	45	45
	Heavy	85	85	65

Three scenarios are considered for dual-aircraft trajectory optimization.

- Scenario 1 - Optimization of a B733 trailing an optimized B733 (similar aircraft type)
- Scenario 2 - Optimization of a B733 trailing an optimized B744 (different aircraft type)
- Scenario 3 - Optimization of a B744 trailing an optimized B733 (different aircraft type)

Results of all the scenarios are discussed in detail. The scenarios are chosen to highlight the behavior of the separation algorithm for different aircraft types, aircraft combinations and the initially assumed time lag Δt. In the figures for dual-aircraft trajectory optimization, there is no clear distinction between the end of phase 1 and start of phase 2 because the conditions for both phases of the trailing aircraft are similar to that of the leading aircraft. It also helps in representing the results in a much simpler and cleaner manner.

5.2.1 Scenario 1 - Optimization of a B733 Trailing an Optimized B733

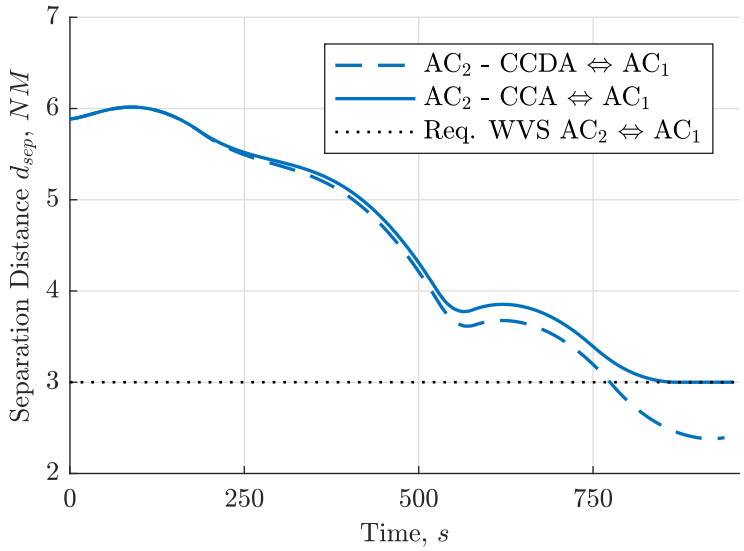

Figure 5.4: Separation distance d_{sep} between the leading aircraft AC1 (B733) and the trailing aircraft AC2 (B733), with an initially assumed time lag Δt of 45 *s*.

The variation of the separation distance between the leading aircraft AC1 (B733) and the trailing aircraft AC2 (B733) with respect to the flight time is shown in figure 5.4. The abbreviation CCDA for the 'dashed line' legend stands for 'Conventional Continuous Descent Arrival'. CCDA is the term used to represent the trajectory the aircraft will follow without the separation distance constraint (equation 5.6). The abbreviation CCA for the 'solid line' legend stands for 'Capacity Constrained Arrival'. CCA is the term used to represent the trajectory the aircraft will follow due to the influence of the separation distance constraint. An initial time lag Δt of 45 s is assumed. Since the velocity of both aircraft are high initially, the separation distance d_{sep} between them is well above the minimum required WVS. During the later stages of flight, as both aircraft are approaching their terminal velocities, the separation distance d_{sep} between them falls below the minimum required WVS. This implies that the constraint represented by the equation 5.6 is in violation. However, GPOPS manages to successfully separate both aircraft by at least the minimum required WVS.

The altitude and CAS profiles of both aircraft are shown in figure 5.5. The profiles of the trailing aircraft AC2 are represented *with* the initially assumed time lag Δt of 45 *s*. For the purpose of comparison, it is useful to plot the altitude and velocity profiles *without* the initially assumed time lag Δt of 45 *s*, as shown in figure 5.6. In order to ensure sufficient separation distance d_{sep},

1) the trailing aircraft AC2 starts its deceleration from a velocity of 250 *kts* earlier than the leading aircraft AC1 and 2) during the last 100 *s* of the flight, the trailing aircraft AC2's deceleration to it's terminal velocity is slower than the leading aircraft AC1 as shown in figure 5.6b. This in turn translates to more separation distance d_{sep} between the two aircraft as shown in figure 5.4.

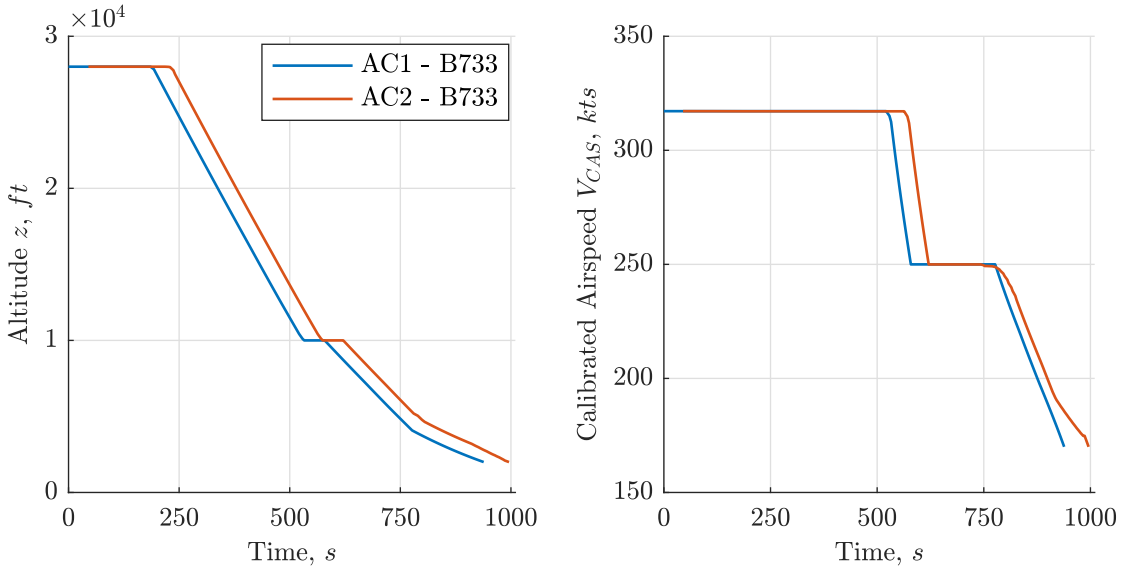

(a) **(b)**

Figure 5.5: Optimization of AC2 (B733) trailing an optimized AC1 (B733), plotted with the initially assumed time lag Δt of 45 *s*. (a) Altitude profile, (b) Calibrated Air Speed profile.

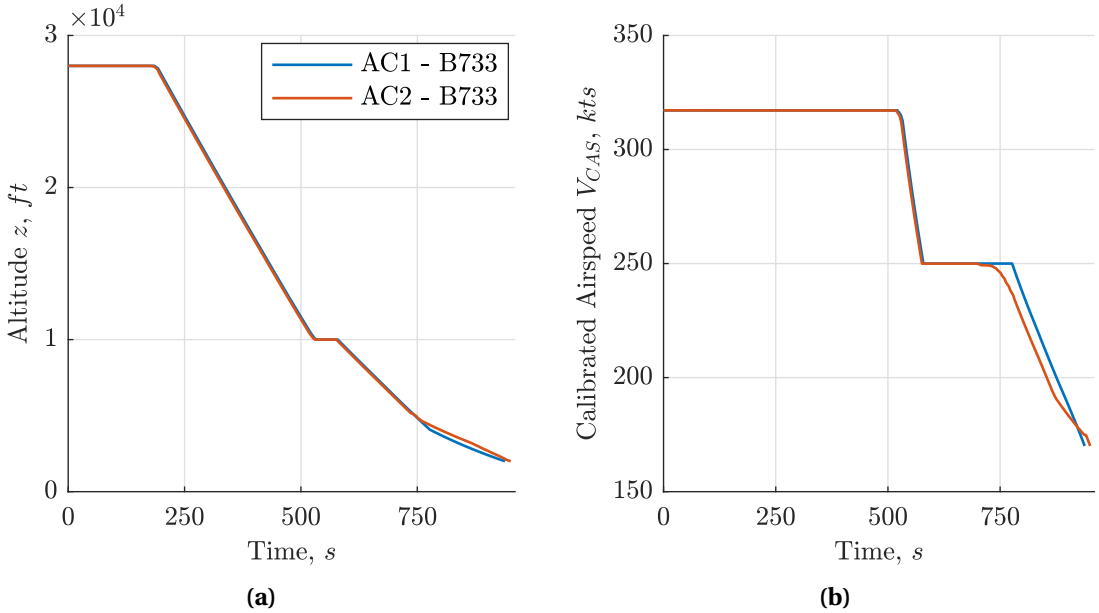

(a) **(b)**

Figure 5.6: Optimization of AC2 (B733) trailing an optimized B733 aircraft, plotted without the initially assumed time lag Δt of 45 *s*. (a) Altitude profile, (b) Calibrated Air Speed profile.

The reduced CAS and slower deceleration of the trailing aircraft AC2 affects it's flight time when compared with the leading aircraft AC1. The variation in the flight time of the trailing aircraft AC2 for varying values of initially assumed time lag Δt are presented in table 5.6. If the initially assumed time lag Δt is large enough to ensure that there is always at least 3 *NM* separation distance between the two aircraft along the entire trajectory, the flight time of the leading aircraft

AC1 and the trailing aircraft AC2 will be equal. If the initially assumed time lag Δt is reduced, the trailing aircraft AC2 will be in conflict with the leading aircraft AC1, forcing it to reduce it's CAS and decelerate slower to satisfy the separation constraint and maintain the minimum required WVS. Additionally, it can be observed that the flight time and delay with CCA are inversely proportional to the initially assumed time lag Δt.

Table 5.6: Variation in flight time for different values of initially assumed time lag Δt.

INITIAL ASSUMED TIME LAG Δt (s)	MINIMUM d_{sep} B/W AC WITH CCDA (NM)	FLIGHT TIME OF THE TRAILING AIRCRAFT AC2 (s)	DELAY WITH CCA (s)
60	>3	938	0
55	2.89	941	3
45	2.38	951	13
35	1.86	961	23
30	1.59	966	27

5.2.2 SCENARIO 2 - OPTIMIZATION OF A B733 TRAILING AN OPTIMIZED B744

Optimization of different aircraft types is not as straightforward as optimization of similar aircraft types. The closer the initial guess is to the final optimal solution, the faster the convergence is to the optimal solution. Due to different performance characteristics of the two aircraft types in consideration, the optimal solution of the leading aircraft AC1 (B744) as an initial guess for the trailing aircraft AC2 (B733) results in longer computation time.

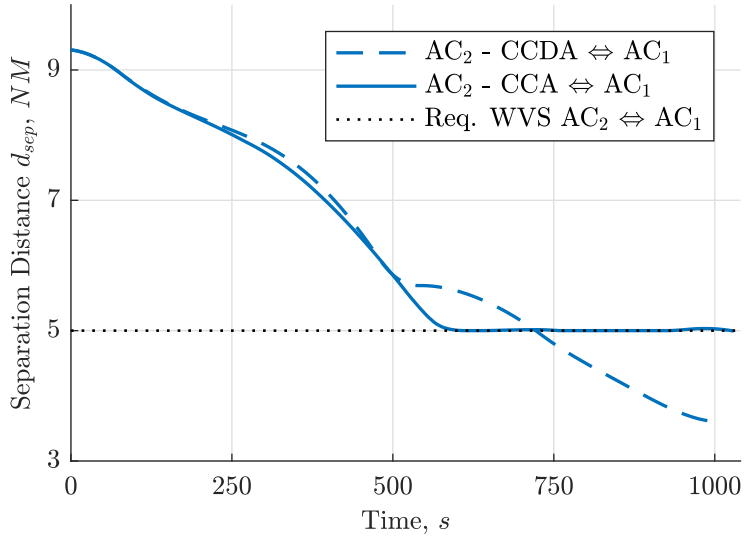

Figure 5.7: Separation distance d_{sep} between the leading aircraft AC1 (B744) and the trailing aircraft AC2 (B733), with an initially assumed time lag Δt of 70 s.

The variation of the separation distance d_{sep} between the leading aircraft AC1 (B744) and the trailing aircraft AC2 (B733) with respect to the flight time is shown in figure 5.7. The optimizer ensures that the trailing aircraft AC2 (B733) is separated with the leading aircraft AC1 (B744) by at least 5NM. The altitude and CAS profiles of both aircraft plotted without the initially assumed time lag Δt of 70 s are shown in figure 5.8. Although the trailing aircraft AC2 (B733) is faster than the leading aircraft AC1 (B744), it is not possible for it to overtake the leading aircraft AC1 (B744)

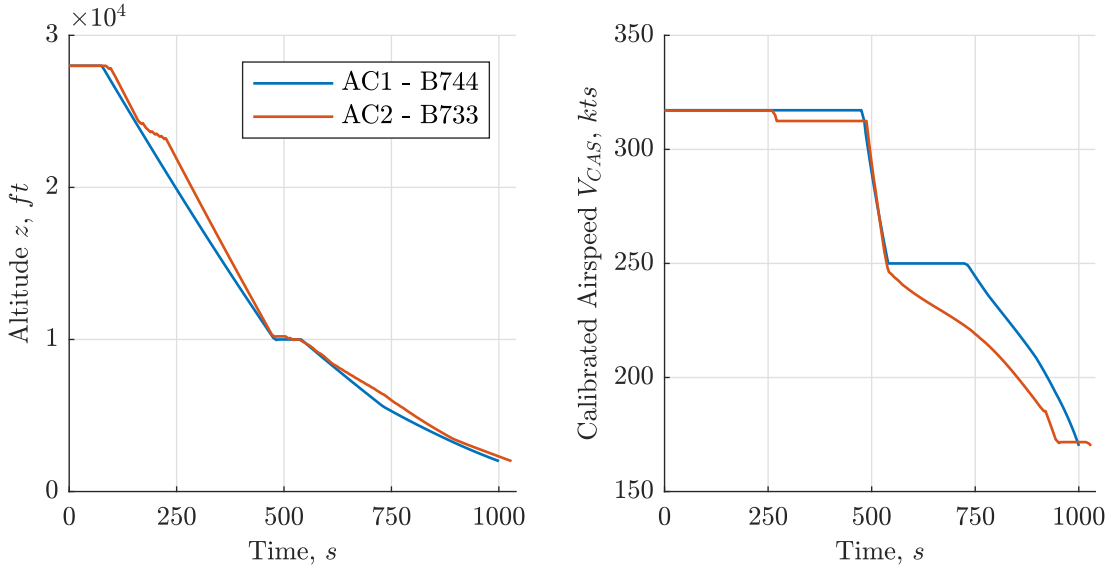

Figure 5.8: Optimization of AC2 (B733) trailing an optimized AC1 (B744) plotted without the initially assumed time lag Δt of 70 *s*. (a) Altitude profile, (b) Calibrated Air Speed profile.

and land before. Even if such a scenario would be possible, the trailing aircraft AC2 (B733) will have to accelerate during the descent phase and compensate for the initially assumed time lag Δt, manage to separate itself from the leading aircraft AC1 (B744) behind it by the minimum required WVS and maintain a vertical separation of at least 1000 *ft*. Assuming that the trailing aircraft AC2 (B733) is allowed to accelerate, with the specified initial and final conditions (table 5.1) and the additional vertical separation constraint, the problem might be infeasible. In a real-time environment, if two aircraft are arriving from the same direction, it would be possible for the trailing aircraft to land first only if it is vectored along a different lateral path.

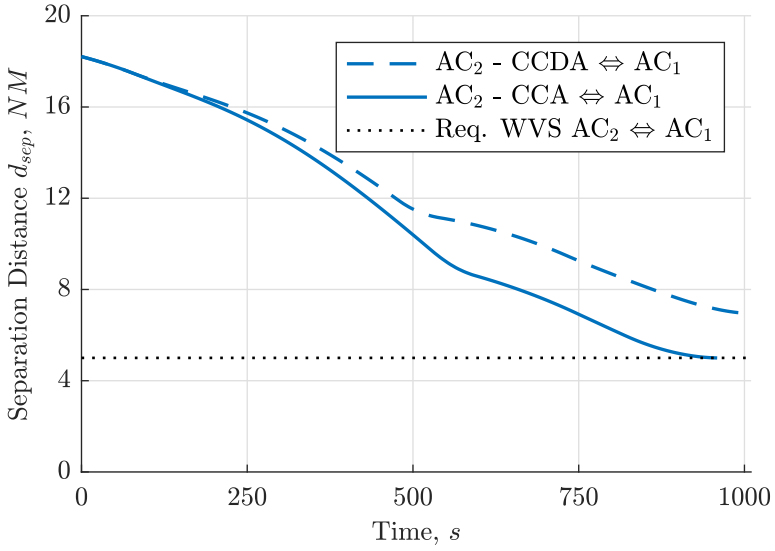

Figure 5.9: Separation distance d_{sep} between the leading aircraft AC1 (B744) and the trailing aircraft AC2 (B733), with an initially assumed time lag Δt of 140 *s*.

Having ruled out the possibility of the trailing aircraft AC2 (B733) landing ahead of the leading aircraft AC1 (B744), figure 5.8b shows that the trailing aircraft AC2 (B733) is forced to reduce it's CAS and decelerate slower than the leading aircraft AC1 (B744) to reach the terminal point after it. The trailing aircraft AC2 (B733) is also forced to maintain it's trajectory closer to that of the

leading aircraft AC1 (B744), although it's trajectory would be different without the separation distance constraint.

It is possible to assume a scenario in which the initially assumed time lag Δt is such that there is no separation constraint violation with the CCDA. However, due to the trailing aircraft AC2 (B733) being inherently faster than the leading aircraft AC1 (B744), during optimization, the two aircraft come in conflict and the separation constraint is violated. This results in the reduction of separation distance between the two aircraft to the minimum required WVS, as shown in figure 5.9.

5.2.3 Scenario 3 - Optimization of a B744 Trailing an Optimized B733

In this scenario, during CCDA, the trailing aircraft AC2 (B744) is slower than the leading aircraft AC1 (B733) along the same pre-defined lateral path by 62 *s*. The initial guess of an optimized B744 aircraft is initiated for the optimization of the trailing aircraft AC2 (B744).

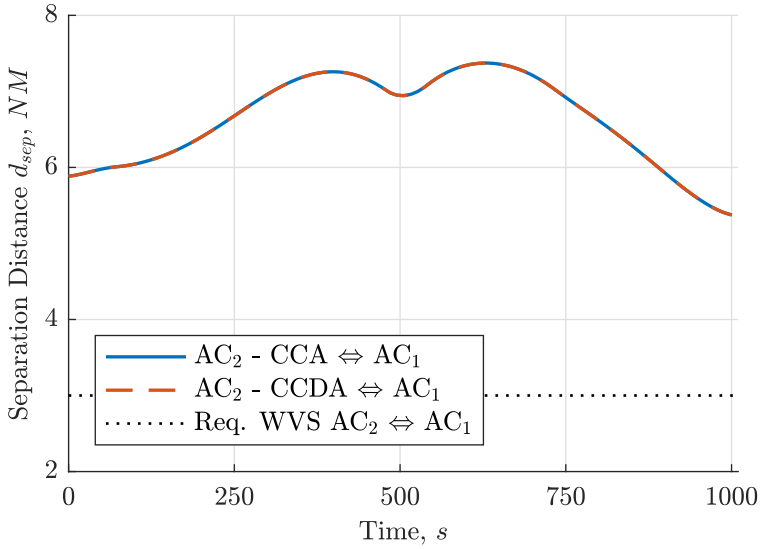

Figure 5.10: Separation distance d_{sep} between the leading aircraft (B733) and the trailing aircraft (B744), with an initially assumed time lag Δt of 45 *s* and, the initial guess of an optimized B744 aircraft.

The variation of the separation distance d_{sep} (equation 4.25) with respect to the flight time is shown in figure 5.10. As a result of the trailing aircraft AC2 (B744) being inherently slower than the leading aircraft AC1 (B733), the separation distance d_{sep} between the two aircraft is higher at all time steps, when compared with previous two scenarios (figures 5.4 and 5.7). The separation distance d_{sep} between them is only a function of the initially assumed time lag Δt, resulting in an initial separation distance d_{sep} of approximately 6 *NM* in this scenario. This also implies that the initially assumed time lag Δt can be reduced even further as it has no effect on the optimization, as long as the initial separation distance d_{sep} between them is greater than the minimum required WVS of 3 *NM*. As both aircraft approach their terminal velocity, the increasing time separation between them ensures that the separation distance d_{sep} is always greater than 6 *NM* (except the last 100 *s* of the flight). Hence, the separation distance constraint (equation 5.6) is never violated and is redundant in this scenario. It can also be observed from this figure that the CCDA and CCA separation distance profiles are overlapping. It results in the flight time of the trailing aircraft AC2 (B744) never being affected by the initially assumed time lag Δt. In other words, the trailing aircraft AC2 (B744) follows a CCDA. At the terminal point, the time separation between the two aircraft is equal to 107 *s*, which is the sum of flight time difference of 62 *s* and

the initially assumed time lag Δt of 45 s.

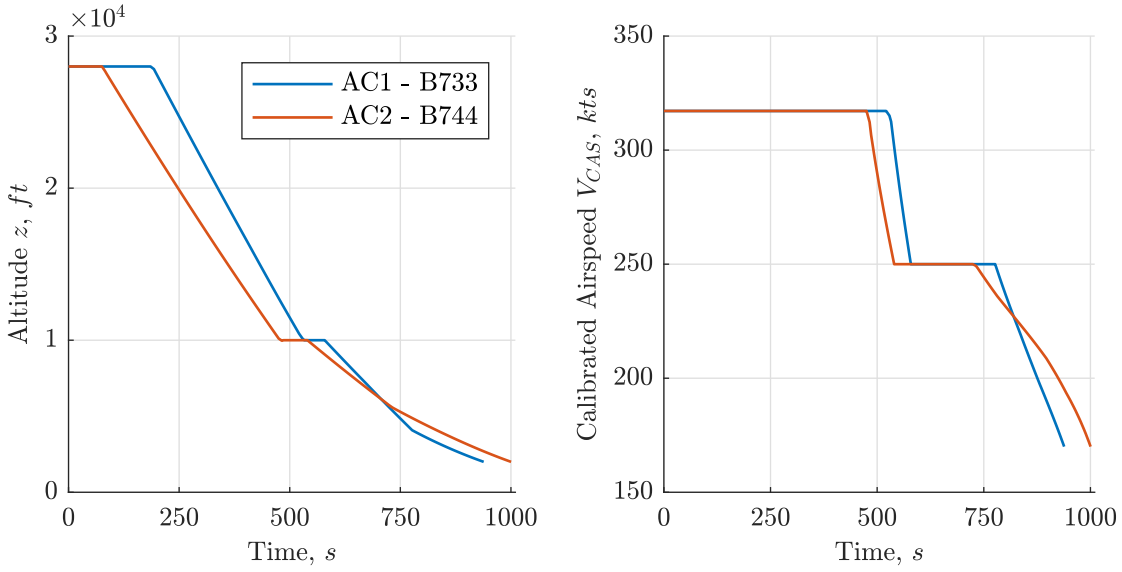

Figure 5.11: Optimization of AC2 (B744) trailing an optimized AC1 (B733) plotted without the initially assumed time lag Δt of 45 s. (a) Altitude profile, (b) Calibrated Air Speed profile.

Unlike in scenario 2 (section 5.2.2), the descent profile of the trailing aircraft AC2 (B744) is independent of the descent profile of the leading aircraft AC1 (B733), as shown in figure 5.11a and can be attributed to the varying performance characteristics of each aircraft and the redundant separation distance constraint (equation 5.6).

5.3 Dual-Aircraft Trajectory Optimization - Different Lateral Path

Having obtained satisfactory results from dual-aircraft trajectory optimization along the same lateral path, aircraft trajectory optimization along two different lateral paths is considered. For this purpose, a new lateral path is designed. The aircraft approaches from the West to the runway 18R and terminates at the FAF after passing through the waypoint EH608. This path is referred to as West-18R. It must be noted that the design of the lateral path West-18R results in an effective distance d_e of 177.05 km. Hence, the lateral path shown in figure 5.1, hereinafter referred to as East-18R, is also extended to ensure that aircraft cover the same effective distance d_e along the two lateral paths. The two lateral paths merge at the waypoint EH608 before reaching the FAF. The optimizer has to ensure that the aircraft are separated by the minimum required WVS only from the merging point until the FAF. The two lateral paths in consideration are represented in figure 5.12.

It must also be noted that in certain cases, it is advantageous to provide an upper and lower limit for the initial effective distance d_e and let the optimization choose the best distance to optimize the vertical trajectory of the aircraft. In such a scenario, if the effective distance d_e travelled by the aircraft is more or less than the pre-calculated lateral path's effective distance d_e, the surplus or deficit distance δd is added before or after the initial starting point i.e., $(x_1 \pm \delta x_1,\ y_1 \pm \delta y_1)$ respectively. This surplus or deficit distance δd is referred to as *path extension* or *path shortening* respectively. This might be an alternate method to a conventional ATC approach in which the aircraft are vectored on different lateral paths to maintain sufficient separation. In figure 5.12, path extension is implemented to extend the lateral path of East-18R from 173.45 km to 177.05 km.

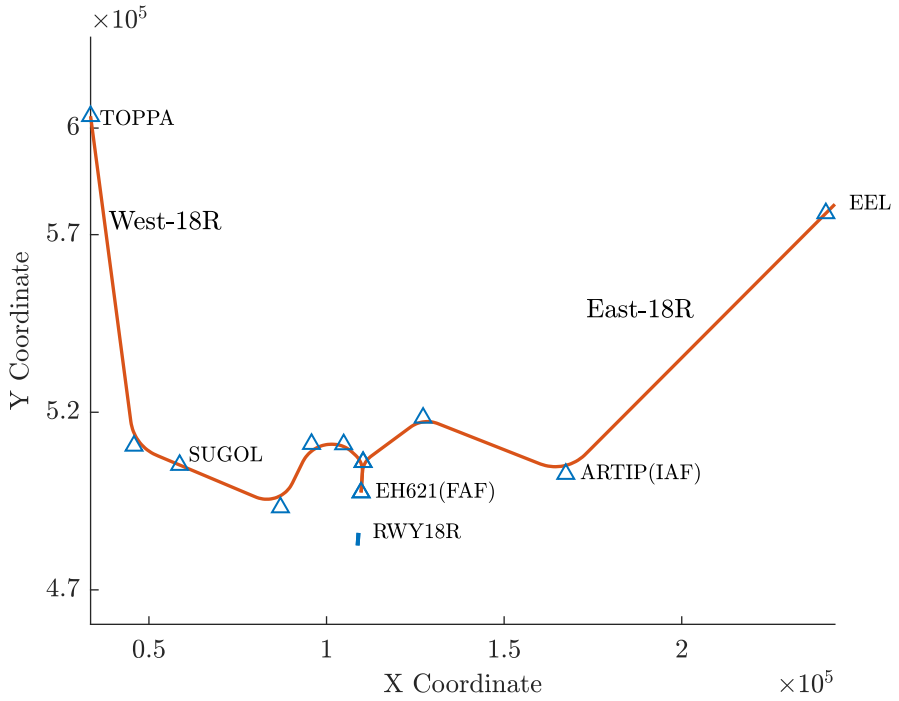

Figure 5.12: Lateral path followed by aircraft arriving from the East and the West to the runway 18R and merging at waypoint EH608 (not labeled) before terminating at the FAF. All units in *m*.

In dual-aircraft trajectory optimization along the same lateral path, it was not possible to consider a scenaio wherein two aircraft enter the sector with a gap of < 10 *s*. If the trailing aircraft AC2 enters the sector after 5 *s* along the same lateral path, for example, it would imply that the initial separation between them is already less than the minimum required WVS. With two aircraft arrive from two different directions (the East and the West), it is feasible to consider a scenario wherein the initially assumed time lag Δt is < 10 *s*. The following scenarios are considered to illustrate the effect of assuming an initial time lag Δt of < 10 *s*,

- Scenario 4 - Optimization of a B744 trailing an optimized B738
- Scenario 5 - Optimization of a B733 trailing an optimized B738

5.3.1 Scenario 4 - Optimization of a B744 Trailing an Optimized B738

In this scenario, the leading aircraft AC1 (B738) is optimized along the lateral path - West-18R. It is assumed that the trailing aircraft AC2 (B744) arrives along the lateral path - East-18R - after just one second i.e., the initially assumed time lag Δt is 1 *s*. In a real-time environment it would imply that both aircraft rougly arrive in the sector at the same time.

The variation of the separation distance d_{sep} between AC1 and AC2 with respect to the flight time is shown in figure 5.13. For better clarity, the separation distance between the leading aircraft AC1 and the trailing aircraft AC2 is shown from 40 *NM*, although the initial separation distance is around 110 *NM*. The separation distance constraint violation only occurs at the merging point, towards the end of the flight. The minimum separation distance between the two aircraft in the CCDA is equal to 0.02 *NM*. In the CCA, the optimizer successfully separates the two aircraft with the minimum required WVS at the expense of significantly reducing the CAS and slowing down the deceleration of the trailing aircraft AC2 to reach it's terminal velocity, as shown in figure 5.14b. Although the initially assumed time lag Δt is 1 *s*, due to the reduced CAS and the slower deceleration of the trailing aircraft AC2, at the terminal point, both aircraft are separated by 58 *s*.

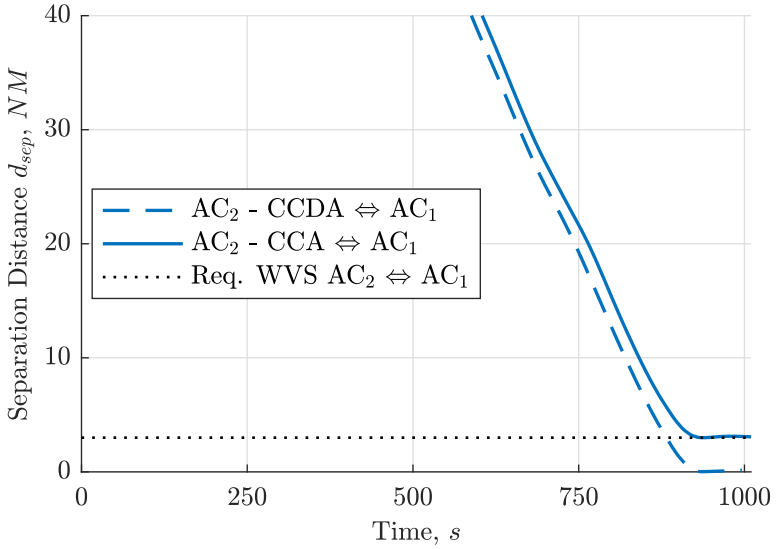

Figure 5.13: Separation distance d_{sep} between the leading aircraft AC1 (B738) and the trailing aircraft AC2 (B744), with an initially assumed time lag Δt of 1 *s*.

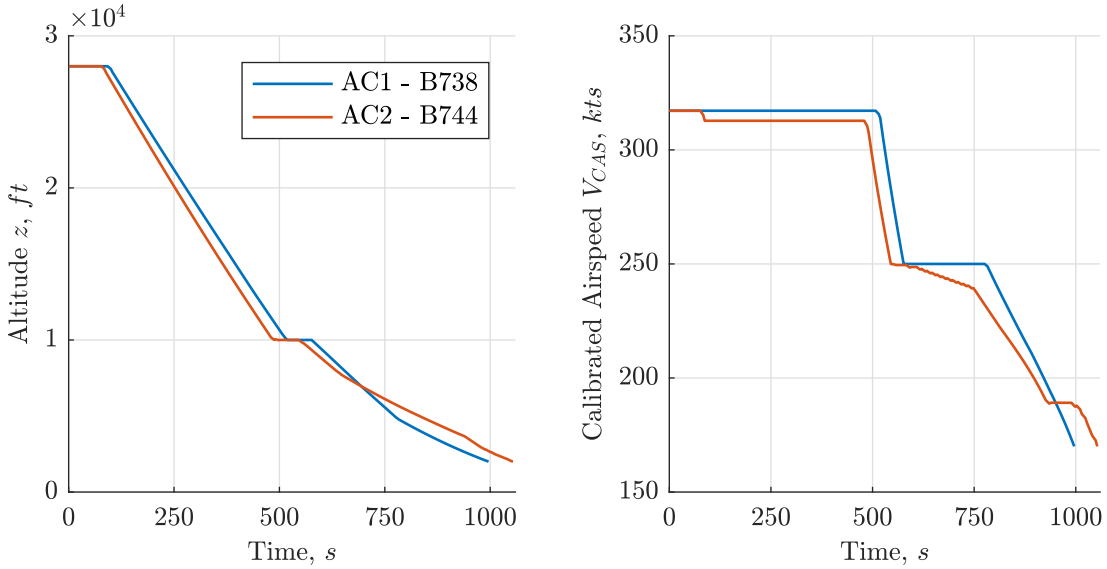

(a) **(b)**

Figure 5.14: Optimization of AC2 (B744) trailing an optimized AC1 (B738) plotted with the initially assumed time lag Δt of 1 *s*. (a) Altitude profile, (b) Calibrated Air Speed profile.

5.3.2 Scenario 5 - Optimization of a B733 Trailing an Optimized B738

It has already been established that a B733 aircraft is faster than all other aircraft types. It is common in ATC practise to make certain trailing aircraft land ahead of the leading aircraft although it enters the sector little later. This is commonly achieved through vectoring. In this scenario, the leading aircraft AC1 (B738) is assumed to enter the sector first and optimized to follow a CCDA along the lateral path - West-18R. Although the initially assumed time lag Δt is 0 *s*, the trailing aircraft AC2 (B733) entering the sector along the lateral path - East-18R - is optimized after the leading aircraft AC1 (B738). Without incorporating any path shortening, the trailing aircraft AC2 (B733) will land after the leading aircraft AC1 (B738), similar to what is noticed in scenario 4.

In order to enable the trailing aircraft AC2 (B733) to land ahead of the leading aircraft AC1 (B738),

the optimizer is free to choose a shorter path i.e., path shortening. Hence, the limits for effective distance d_e to be travelled by the aircraft in phase 1 are redefined as,

$$0 \leq d_e^{(1)} \leq d_{min} \tag{5.7}$$

$$\& \quad 5 \leq d_e^{(1)} \leq d_{max} \tag{5.8}$$

where d_e is the effective distance in *NM*. The optimizer is free to choose any initial distance between 0 and 5 *NM*.

If the optimizer chooses to shorten the path of the trailing aircraft AC2 (B733), it will induce a *penalty* on the objective function value. The penalty parameter is defined as,

$$J_{pen} = \left(\frac{\Delta d}{V}\right)^{1.5} \tag{5.9}$$

where Δd in m is the shortened path of the trailing aircraft AC2 (B733) and V is the velocity and is choosen to be 100 ms^{-1}. The penalty is raised to the power 1.5 to make it exponential and also ensure that the penalty on the objective function is not too high for a given value of Δd. A power higher than 1.5 would result in a large penalty on the objective function value, forcing the optimizer to land the trailing aircraft AC2 (B733) behind the leading aircraft AC1 (B738).

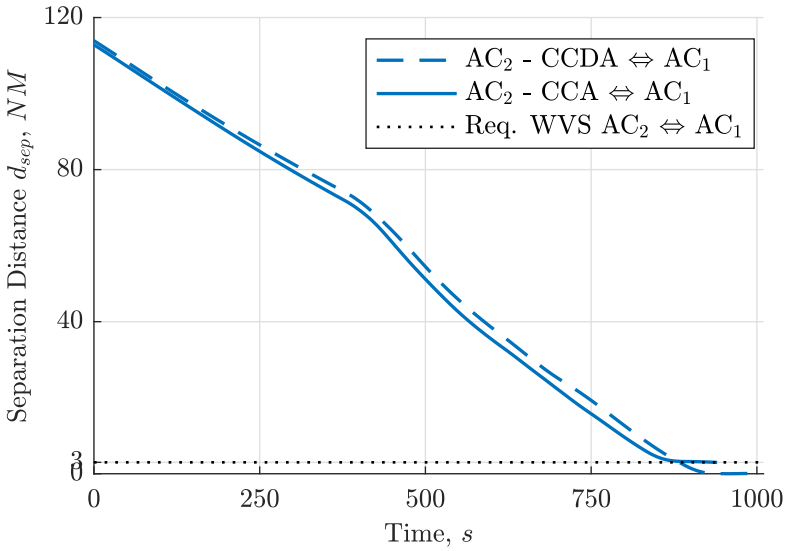

Figure 5.15: Separation distance d_{sep} between the leading aircraft AC1 (B738) and the trailing aircraft AC2 (B733), with an initially assumed time lag Δt of 0 *s*.

The variation of the separation distance d_{sep} between the leading aircraft AC1 (B738) and the trailing aircraft AC2 (B733) with respect to the flight time is shown in figure 5.15. It can be observed that the minimum separation distance between the leading aircraft AC1 (B738) and the trailing aircraft AC2 (B733) with CCDA is equal to 0 *NM*. In the CCA, the trailing aircraft AC2 (B733) is separated with the leading aircraft AC1 (B738) by the minimum required WVS of 3 *NM*. The altitude and CAS profile of the two aircraft are shown in figure 5.16. It can be observed that the fight time of the trailing aircraft AC2 (B733) is much shorter than the leading aircraft AC1 (B738). This implies that the trailing aircraft AC2 (B733) has landed before the leading aircraft AC1 (B738). Table 5.7 shows the comparison of flight time and objective function value of both aircraft. It can be observed that due to the path shortening of 3.2 *km*, the trailing aircraft AC2 (B733) incurs a penalty on the objective function equal to 181.6 *s*. The shortened effective distance d_e of the trailing aircraft AC2 (B733) also results in a shorter flight time by 12 *s*.

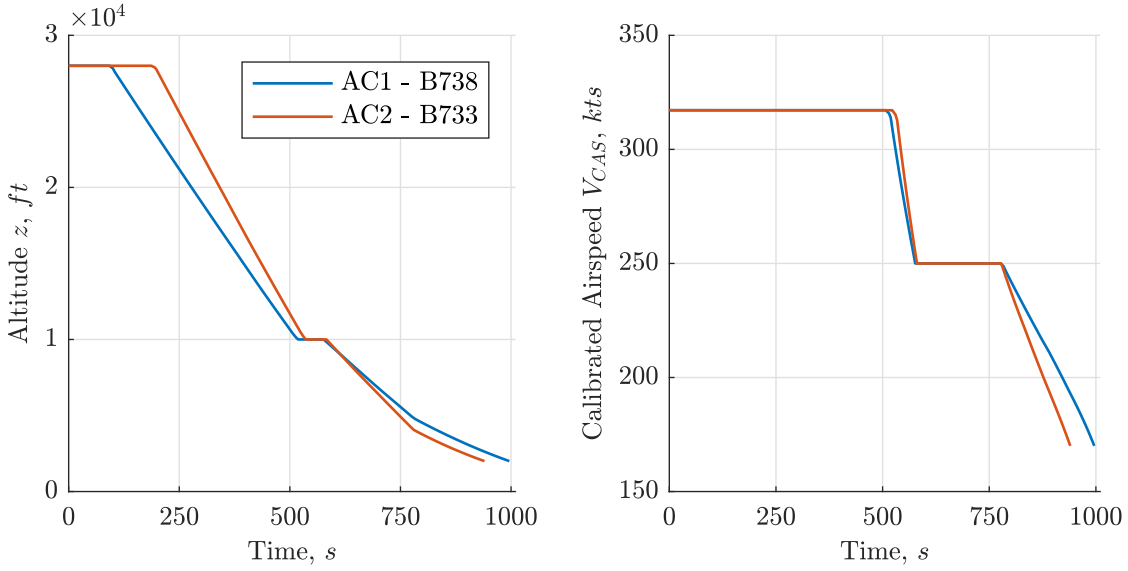

Figure 5.16: Optimization of AC2 (B733) trailing an optimized AC1 (B738) plotted with the initially assumed time lag Δt of 0 *s*. (a) Altitude profile, (b) Calibrated Air Speed profile.

Table 5.7: Comparison of flight time and objective function value in scenario 5.

AC NO. & TYPE	EFFECTIVE DISTANCE (km)	FLIGHT TIME (s)	OBJECTIVE FUNCTION VALUE
AC1 - B738	177.048	996.17	996.17
AC2 - B733	173.841	939.97	1121.58

Scenario 5 is also applicable for a B744-B733 aircraft pair. Table 5.8 compares the objective function value and flight time of a B744-B733 aircraft pair. Although the trailing aircraft AC2 (B733) lands before the leading aircraft AC1 (B744), there is no path shortening of the trailing aircraft AC2 (B733). This is because a B744 aircraft is even slower than a B738 aircraft by approximately 15 *s*.

Table 5.8: Comparison of flight time and objective function for a B744-B733 aircraft pair.

AC NO. & TYPE	EFFECTIVE DISTANCE (km)	FLIGHT TIME (s)	OBJECTIVE FUNCTION VALUE
AC1 - B744	177.048	1015.05	1015.05
AC2 - B733	177.048	952	952

5.4 MULTI-AIRCRAFT TRAJECTORY OPTIMIZATION - DIFFERENT LATERAL PATH

The aircraft separation algorithm, discussed in section 4.4.1, is extended for multi-aircraft trajectory optimization with a few additions. Firstly, when the third aircraft AC3, for example, enters the sector, it is ensured that the third aircraft AC3 maintains separation distance d_{sep} not only with the second aircraft AC2, but also with the first aircraft AC1. This is because when the third aircraft (AC3) is closer to the final approach path (last 100-200 *s* of flight), the first aircraft AC1 is still on the glideslope path. The minimum required WVS separation between AC1 and

AC3 ($d_{WVS_{1-3}}$) is the sum of minimum required WVS between AC1 and AC2 ($d_{WVS_{1-2}}$) and, AC2 and AC3 ($d_{WVS_{2-3}}$).

$$d_{WVS_{1-3}} = d_{WVS_{1-2}} + d_{WVS_{2-3}} \tag{5.10}$$

Secondly, the initially assumed time lag between AC1 and AC3 (Δt_{1-3}) is the sum of the initially assumed time lag between AC1 and AC2 (Δt_{1-2}) and, AC2 and AC3 (Δt_{2-3}).

$$\Delta t_{1-3} = \Delta t_{1-2} + \Delta t_{2-3} \tag{5.11}$$

A similar approach can be extended for all trailing aircraft (AC4, AC5, etc.) entering the sector. It is sufficient for any trailing aircraft to maintain the minimum required WVS with only two aircraft ahead of it. This is because when the third aircraft AC3 is at the terminal point, the first aircraft AC1 would have already landed. Therefore, it is no longer required for the fourth aircraft AC4 to maintain separation with the first aircraft AC1. Hereinafter, when more than three aircraft are being optimized, only the separation distance d_{sep} between the aircraft currently being optimized and the two aircraft ahead of it will be depicted.

5.4.1 Scenario 6 - Optimization of 10 Aircraft Sequence

More aircraft can be added to the two different lateral paths - West-18R and East-18R. In this scenario up to 10 aircraft are considered, the aircraft sequence and the lateral path followed by them are shown in table 5.9, and is chosen at random.

The scenario is designed such that every trailing aircraft is always in conflict with one or two aircraft that are ahead of it. The initially assumed time lag Δt derived from table 5.5 ensures that the difference between the minimum required WVS and the minimum separation distance between any of the trailing aircraft and the aircraft ahead of it (with violation) is always $< 1\ NM$.

Table 5.9: Aircraft sequence for scenario 6.

Aircraft no. & Type	Lateral Path	Sector Entering Time (s)	Minimum required WVS with previous AC (NM)
AC1 - B733	East-18R	0	-
AC2 - B738	West-18R	45	3
AC3 - B738	East-18R	90	3
AC4 - B744	East-18R	135	3
AC5 - B738	West-18R	220	5
AC6 - MD11	East-18R	265	3
AC7 - MD11	West-18R	330	4
AC8 - B738	West-18R	415	5
AC9 - B738	East-18R	460	3
AC10 - B744	West-18R	505	3

It can be noted from table 5.5 that,

$$\Delta t_{1-2} = 45\ s \tag{5.12}$$

$$\Delta t_{2-3} = 45\ s \tag{5.13}$$

$$\Delta t_{1-3} = 45\ s + 45\ s = 90\ s \tag{5.14}$$

Also, it can be noted from table 5.3 that,

$$d_{WVS_{1-2}} = 3\ NM \tag{5.15}$$
$$d_{WVS_{2-3}} = 3\ NM \tag{5.16}$$
$$d_{WVS_{1-3}} = 3\ NM + 3\ NM = 6\ NM \tag{5.17}$$

A similar approach can be extended for all trailing aircraft entering the sector.

The variation of the separation distance d_{sep} between AC10 and AC9 and, AC10 and AC8 with respect to the flight time is shown in figure 5.17. For better clarity, the separation distance between AC9 and AC10 is shown from 30 *NM*, although the initial separation is around 110 *NM*. It can be observed that AC10 is separated by the minimum required WVS from AC9 as well as AC8.

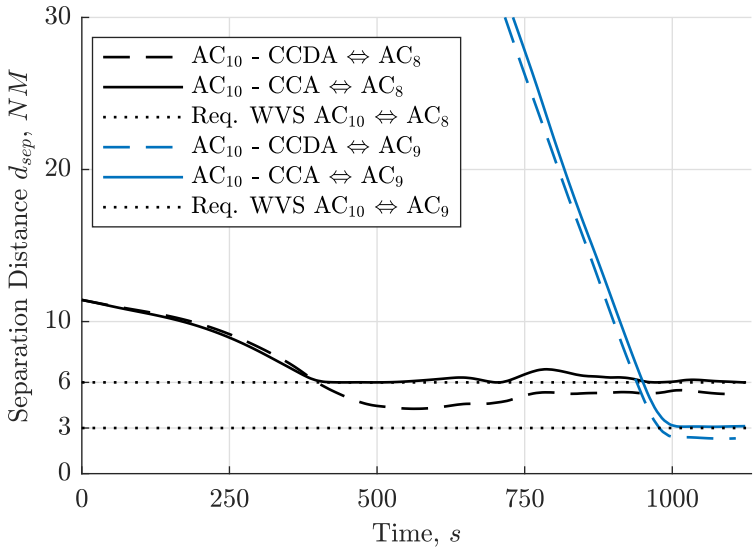

Figure 5.17: Separation distance d_{sep} between AC10 (B744) and AC8 (B738) and, AC10 (B744) and AC9 (B738), with an initially assumed time lag Δt of 90 *s* and 45 *s* respectively.

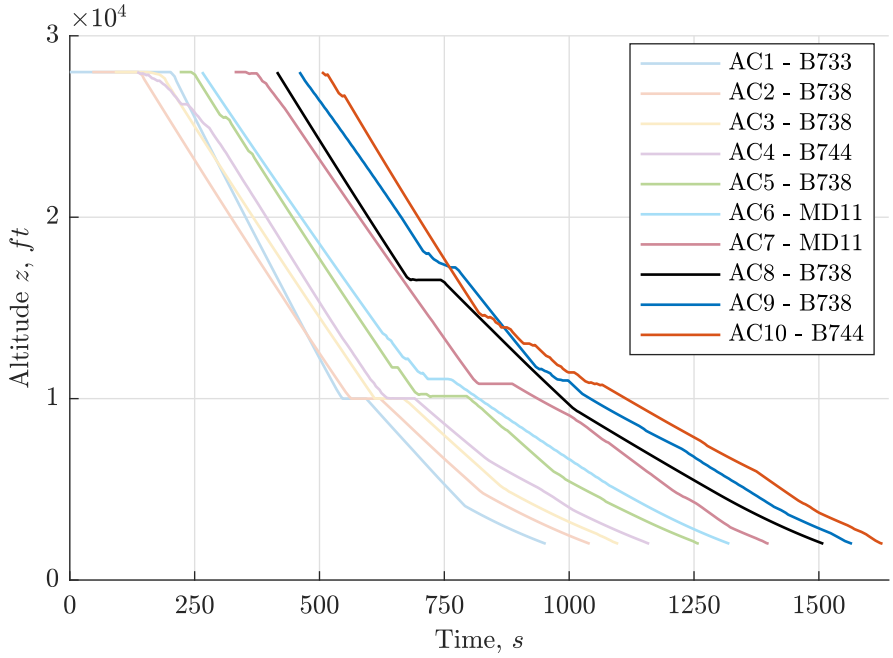

Figure 5.18: Altitude profile of all aircraft plotted with the initially assumed time lag Δt.

The altitude and CAS profiles of all 10 aircraft plotted with the initially assumed time lag Δt are shown in figure 5.18 and 5.19 respectively. Every trailing aircraft CAS is lesser and deceleration slower than the aircraft preceding it. Therefore, the flight time of every trailing aircraft is more than the flight time of the aircraft preceding it. Additionally, the difference in flight time between the CCA and the CCDA also increases gradually as shown in table 5.10. The increasing flight time of CCA also indicates that every trailing aircraft is in conflict with the aircraft ahead of it in a CCDA. When more aircraft are added to this sequence and assuming that they are in conflict with the aircraft ahead of it, at some point, it will no longer be possible to delay the trailing aircraft to maintain sufficient separation, while still being able to satisfy aircraft performance characteristics.

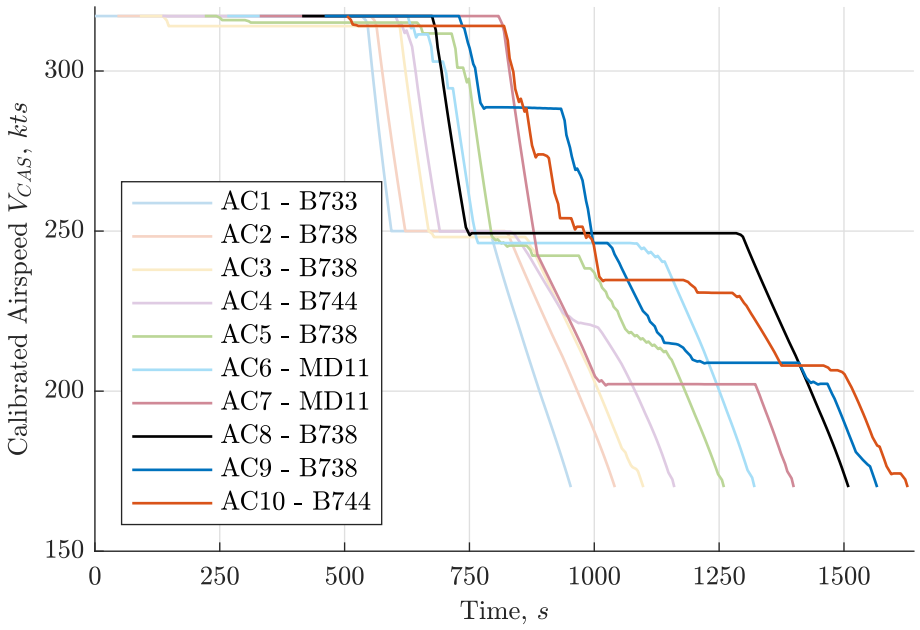

Figure 5.19: Calibrated Air Speed profile of all aircraft plotted with the initially assumed time lag Δt.

Table 5.10: Flight time comparison of all aircraft in scenario 6.

AIRCRAFT NO. & TYPE	LATERAL PATH	FLIGHT TIME - CCDA (s)	FLIGHT TIME - CCA (s)	FLIGHT TIME DIFFERENCE WITH CCDA (s)
AC1 - B733	East-18R	953.06	953.06	0
AC2 - B738	West-18R	996.17	996.17	0
AC3 - B738	East-18R	997.67	1008.19	10.52
AC4 - B744	East-18R	1015.05	1025.24	10.19
AC5 - B738	West-18R	996.17	1039.99	43.82
AC6 - MD11	East-18R	997.28	1056.81	59.53
AC7 - MD11	West-18R	995.01	1072.16	77.15
AC8 - B738	West-18R	996.17	1094.85	98.68
AC9 - B738	East-18R	997.28	1107.38	110.1
AC10 - B744	West-18R	1012.62	1123.32	110.7

The spatial positions of all the 10 aircraft before the start and end of optimization of AC10 are plotted along the two considered lateral paths, as shown in figure 5.20. This figure also illustrates the maintained separation distance between each aircraft at the terminal point.

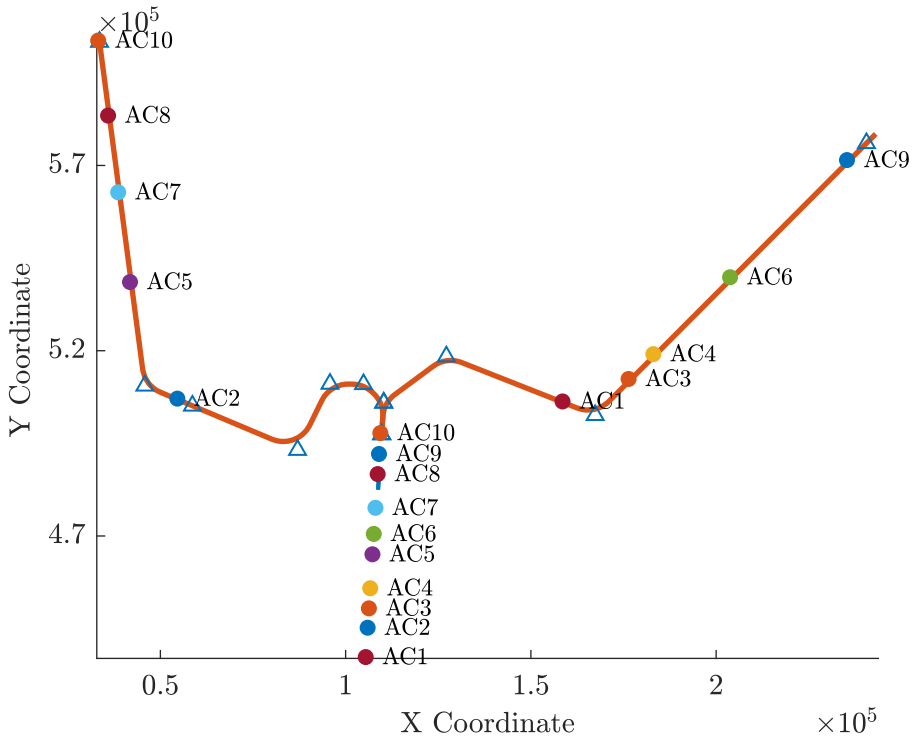

Figure 5.20: Spatial positions of all aircraft at the start and end of optimization of AC10.

5.5 Comparison of Fuel and Time Optimized Trajectories

With airlines increasingly focusing on cutting operational costs, it is important to ensure that the aircraft separation algorithm can also be applied to obtain fuel optimized trajectories. For this scenario, the aircraft sequence along with the required separation distance and the initially assumed time lag Δt is shown in table 5.11.

Table 5.11: Aircraft sequence for comparison of fuel and time optimized trajectories.

AC number	AC Type	Time difference with previous AC (*s*)	Minimum required WVS with previous AC (*NM*)
1	B738	-	-
2	B738	45	3
3	B744	45	3
4	B738	85	5
5	B733	45	3

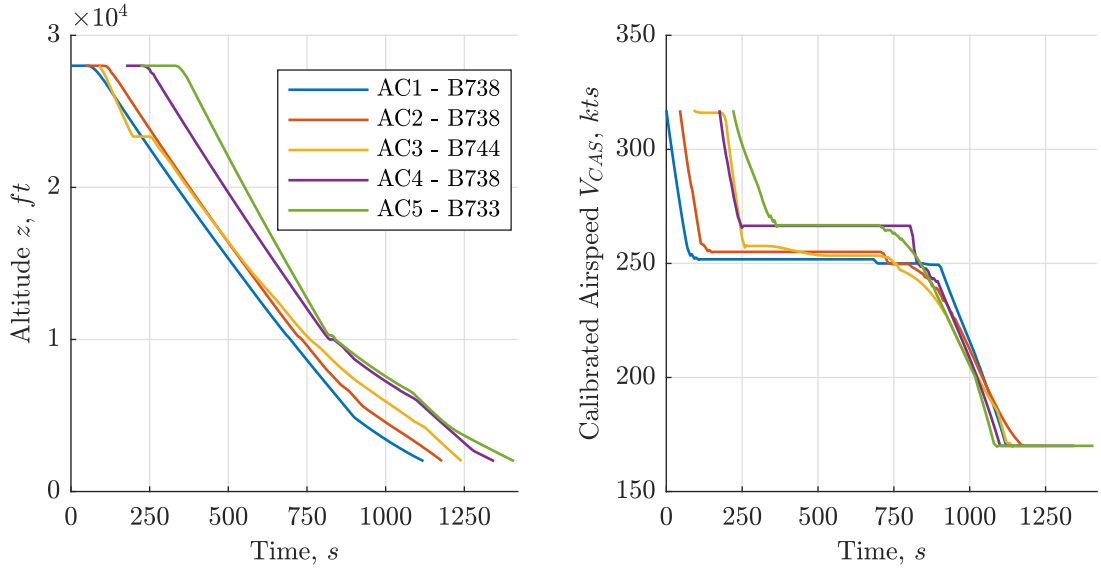

(a) **(b)**

Figure 5.21: Optimized trajectories of all aircraft plotted with the initially assumed time lag Δt. (a) Altitude profile, (b) Calibrated Air Speed profile.

The altitude and CAS profiles of all five aircraft, with the initially assumed time lag Δt are shown in figure 5.21. Fuel optimized trajectories are not very different from time optimized trajectories, but with a single exception. There is no thrust utilized by the aircraft at the initial altitude as shown in figure 5.22a. Although it can be seen from figure 5.21a that aircraft make level segments at initial altitudes, they result in reduction of the CAS of the aircraft at the cost of zero thrust utilized. The CAS of the aircraft is reduced until it reaches the *optimal glide speed* (the speed at which L/D ratio is maximum). Additionally, the optimal glide speed of an aircraft is proportional to it's weight. Among the available aircraft models, the B733 is the lightest and it's optimal glide speed is around 220 *kts*. If a B744 is being optimized behind an optimized B733, the B744 will be forced to slow down more than the B733, although it's glide speed is much higher. The initial loss in the CAS of the aircraft proves to be a disadvantage in optimizing more aircraft. After 4-5 aircraft, it becomes difficult to optimize further incoming aircraft since the velocity cannot be reduced any further. The jitter seen in the thrust profiles of AC2-AC5 can largely be attributed to the Radau methodology.

Table 5.12: Comparison of flight time and fuel consumption for fuel optimized and time optimized trajectories.

Aircraft No.	Fuel Optimized		Time Optimized	
	Fuel Consumed *(kg)*	Flight time *(s)*	Fuel Consumed *(kg)*	Flight time *(s)*
AC1	156.97	1120	212.25	998
AC2	161.55	1134	215.03	1010
AC3	542.97	1151	585.33	1027
AC4	187.62	1170	227.36	1043
AC5	265.01	1188	302.23	1058

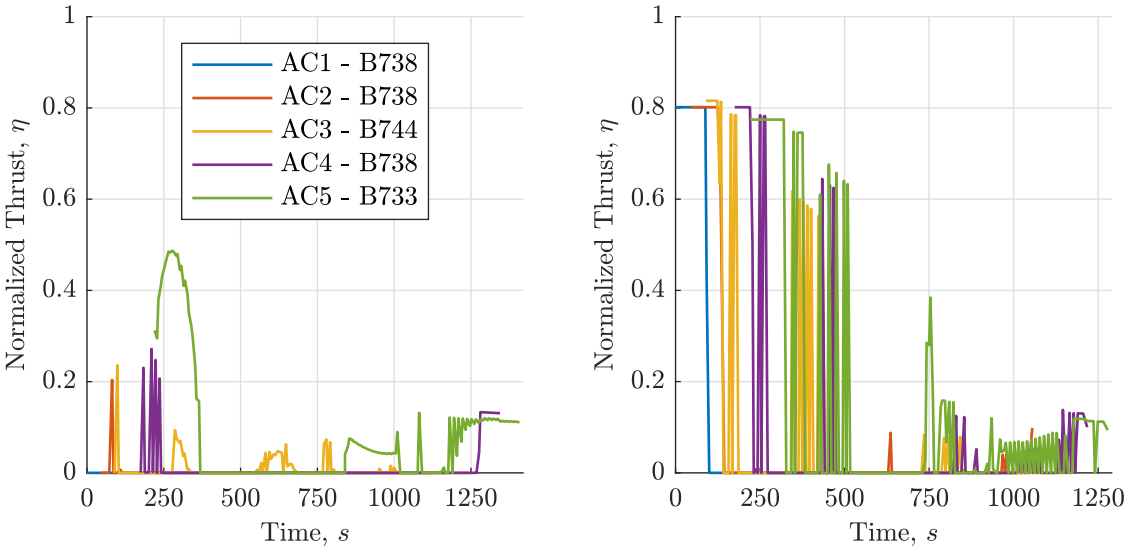

(a) (b)

Figure 5.22: Thrust profiles of the all aircraft plotted with the initially assumed time lag Δt. (a) Fuel optimized, (b) Time optimized.

The initial loss of speed in turn has an effect on the total flight time of fuel optimized trajectories as shown in table 5.12. The flight time and fuel consumed by all aircraft if the same sequence is optimized with respect to time is also shown in this table for comparison. In both time and fuel optimized trajectories it can be observed that the flight time increase progressively due to the trailing aircraft slower deceleration and reduced CAS to satisfy the separation distance constraint. Hence, the fuel consumed by aircraft also increases progressively as the flight time increases. The fuel consumed by aircraft in time optimized trajectories is more because of the level segment made by all aircraft at the initial altitude at the expense of thrust (figure 5.22b).

5.6 Multi-Aircraft Trajectory Optimization - AMS Airport Real-time Data

In order to validate the aircraft separation algorithm for CDAs, AMS airport's real-time inbound flight data is used. The data contains details about all aircraft tracked using RADAR equipment on October 22, 2010. The data provides details about aircraft type, coordinates, flight level, the runway it landed on, sector entering time, etc. This inbound flight data is arranged in the ascending order of aircraft sector entering time. Although the flight level of all aircraft is not the same, but for the purpose of simulation all aircraft are optimized for the same set of initial and final conditions. Also, due to unavailability of various aircraft performance models, other aircraft types are substituted with the available aircraft performance models. For example, an A320 is replaced with a B738, a F70 and a F100 are replaced with a B733, a B777 and a B767 are replaced with a B744 or a MD11, etc.

Due to availablility of coordinate information in the data, it was possible to accertain the direction from which the aircraft enter the sector. For arrivals on the runway 18R and the runway 18C, aircraft enter the sector from three different directions - the East, the West and the South. Hence, a new lateral path arriving from the South to the runway 18R is designed. This path will be referred to as South-18R. All three lateral paths considered for the simulation of real-time data is shown in figure 5.23. The effective distance d_e to be travelled by the aircraft in each of the three lateral paths is equal to 177.05 *km*.

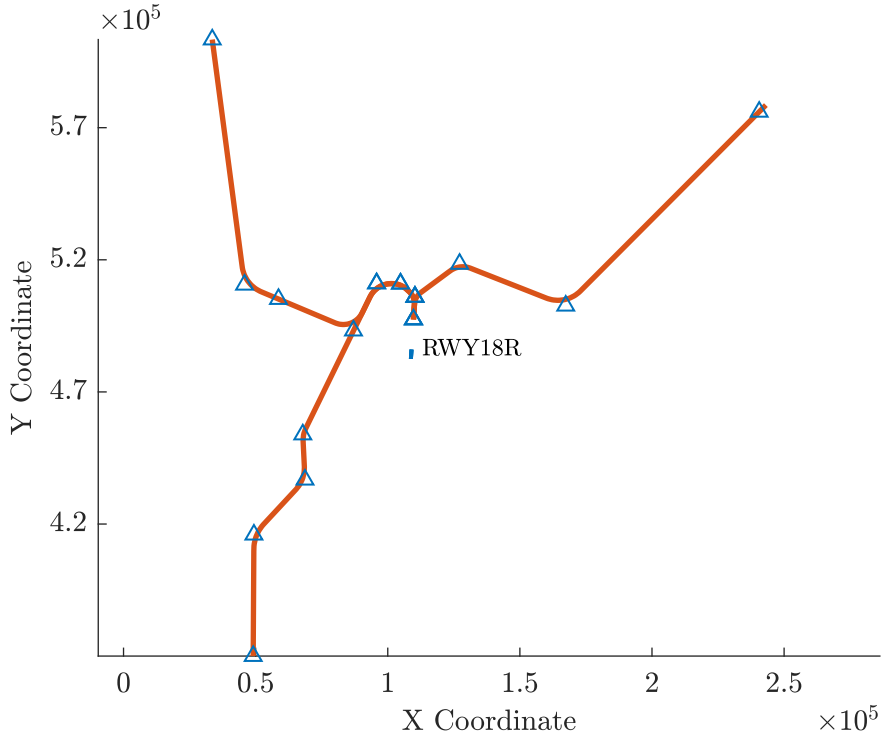

Figure 5.23: The three lateral paths considered for real-time inbound flight data simulation. All units in *m*.

For multi-aircraft trajectory optimization using AMS airport's real-time inbound flight data, the following three scenarios are considered.

- Scenario 7 - Morning arrival peak period (09:11 - 09:20)
- Scenario 8 - Evening end of arrival peak period (17:47 - 18:02)
- Scenario 9 - Evening arrival peak period (16:57 - 17:03)

5.6.1 Scenario 7 - Morning Arrival Peak Period (09:11 - 09:20)

For this scenario, a morning arrival peak period data is considered. Although two arrival runways (18R and 18C) were in use and it was known prior the runway on which the aircraft would land, all aircraft considered in this scenario are simulated to land on the runway 18R only. All information pertaining to the aircraft sequence considered in this scenario is presented in table 5.13. Five aircraft landed on the runway 18R and other aircraft landed on the runway 18C. It can be observed from the time difference (AC3 - AC5 and AC8 - AC10) in table 5.13 that the sequencing will lead to significant shrinkage of space between certain aircraft pairs, resulting in a more constrained problem.

The CAS profiles of all aircraft in this scenario are shown in figure 5.24. It can be noticed that due to the marginal time difference Δt between AC8, AC9 and AC10, the optimizer chooses to significantly reduce the CAS and slow their deceleration to ensure non-violation of the separation distance constraint. This is also reflected in the large flight time difference between the CCDA and the CCA, as shown in table 5.14 for AC8, AC9 and AC10. Significant reduction in the CAS of the aircraft, such as AC10, can have certain disadvantages. Firstly, it results in longer flight time. Secondly, if AC11 is to be introduced in the sector such that it is in conflict with AC9 or AC10, the problem may become infeasible. This is because AC11 will have to reduce it's CAS more and decelerate slower than AC10 to satisfy the separation distance constraint, but after a certain threshold, reducing the CAS of the trailing aircraft any further is not possible while

still being able to maintain aircraft performance characteristics. If AC11 enters the sector after a significantly long time and not be in conflict with AC9 or AC10, then the problem would be feasible. It also facilitates AC11 to regain some speed in comparison with AC10. This effect can be observed with AC7 (Δt of 63). It can be observed from table 5.14 that due to the AC7 being a B744, which is the slowest, coupled with large time difference, ensures that it follows a CCDA.

Table 5.13: Aircraft sequence for scenario 7.

AC NO.	ACTUAL AC TYPE	CHOSEN AC TYPE	DIRECTION	SECTOR ENTERING TIME (*hh:mm:ss*)	TIME DIFFERENCE WITH PREVIOUS AC *(s)*
AC1	A320	B738	East	09:11:31	-
AC2	F100	B733	West	09:12:43	72
AC3	B738	B738	South	09:13:26	43
AC4	B734	B733	West	09:14:19	53
AC5	B738	B738	South	09:14:47	28
AC6	B738	B738	South	09:16:23	96
AC7	B772	B744	South	09:17:26	63
AC8	A320	B738	East	09:17:46	20
AC9	B772	MD11	West	09:18:24	38
AC10	B738	B738	East	09:19:07	43

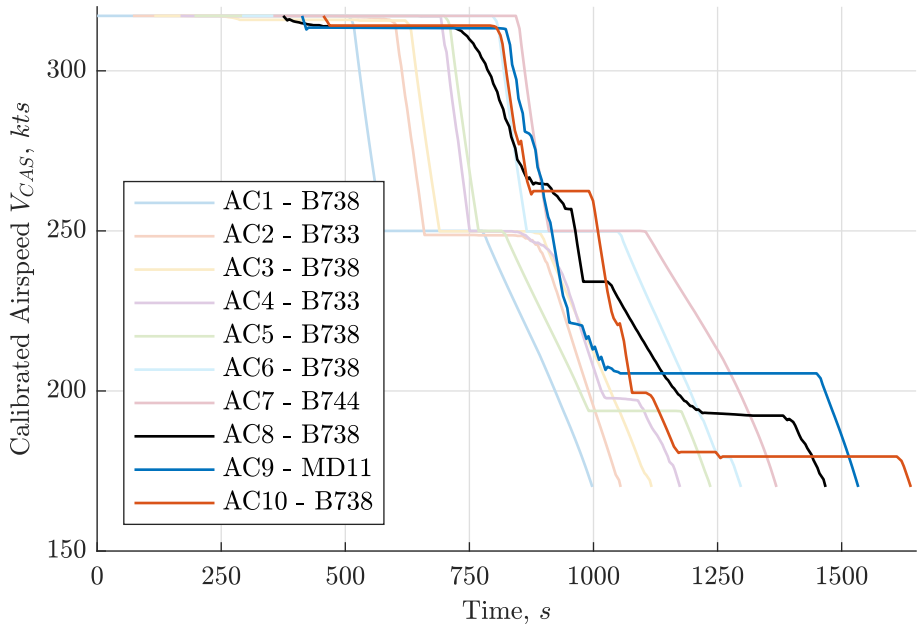

Figure 5.24: Calibrated Air Speed profile of all aircraft plotted with the time difference Δt.

Table 5.14: Flight time comparison of all aircraft in scenario 7.

AIRCRAFT NO. & TYPE	DIRECTION	FLIGHT TIME - CCDA (*s*)	FLIGHT TIME - CCA (*s*)	FLIGHT TIME DIFFERENCE WITH CCDA (*s*)
AC1 - B738	East	997.67	997.67	0
AC2 - B733	West	952	982.71	30.71
AC3 - B738	South	996.92	1002	5.08
AC4 - B733	West	952	1006.25	54.25
AC5 - B738	South	996.92	1039.69	42.77
AC6 - B738	South	996.92	1005.15	8.23
AC7 - B744	South	1013.68	1013.68	0
AC8 - B738	East	997.67	1092.53	94.86
AC9 - MD11	West	995.01	1120.46	125.45
AC10 - B738	East	997.67	1183.30	185.63

5.6.2 SCENARIO 8 - EVENING END OF ARRIVAL PEAK PERIOD (17:47 - 18:02)

Table 5.15: Aircraft sequence for scenario 8.

AC NO.	ACTUAL AC TYPE	CHOSEN AC TYPE	DIRECTION	SECTOR ENTERING TIME (*hh:mm:ss*)	TIME DIFFERENCE WITH PREVIOUS AC (*s*)
AC1	A320	B738	South	17:47:44	-
AC2	B744	B744	East	17:48:19	39
AC3	B744	B744	East	17:49:50	91
AC4	B772	MD11	South	17:53:07	197
AC5	B734	B733	East	17:54:24	77
AC6	F100	B733	East	17:55:41	77
AC7	F70	B733	East	17:57:12	91
AC8	A320	B738	South	17:57:55	43
AC9	A320	B738	West	17:58:58	63
AC10	A320	B738	South	17:59:16	18
AC11	B734	B733	West	18:01:02	106

For this scenario, an end of evening arrival peak is considered. At the end of an arrival peak, the second arrival runway's use is minimised gradually. All information pertaining to the aircraft sequence considered in this scenario is shown in table 5.15. Except for two aircraft i.e., AC2 and AC3, all aircraft landed on the runway 18R. It can be observed from the time difference in table 5.15 that there is sufficient separation between aircraft pairs, resulting in a less constrained problem.

The variation of the separation distance d_{sep} (equation 4.31) between AC11 and two aircraft

ahead of it with respect to the flight time is shown in figure 5.25. For better clarity, the separation distance between the aircraft pairs is shown from 40 *NM*, although the initial separation is around 110 *NM*. The effect of separation distance observed in this figure is similar to what was observed in scenario 2.

The flight time differences between CCDA and CCA in table 5.16 clearly implies that 6 of 11 aircraft follow CCDA. A trailing B733 aircraft (AC5, AC6, AC11) will always result in large flight time difference with CCDA due to the much shorter flight time compared with other aircraft. Hence, a trailing B733 aircraft will always incur more penalty for a given time difference Δt.

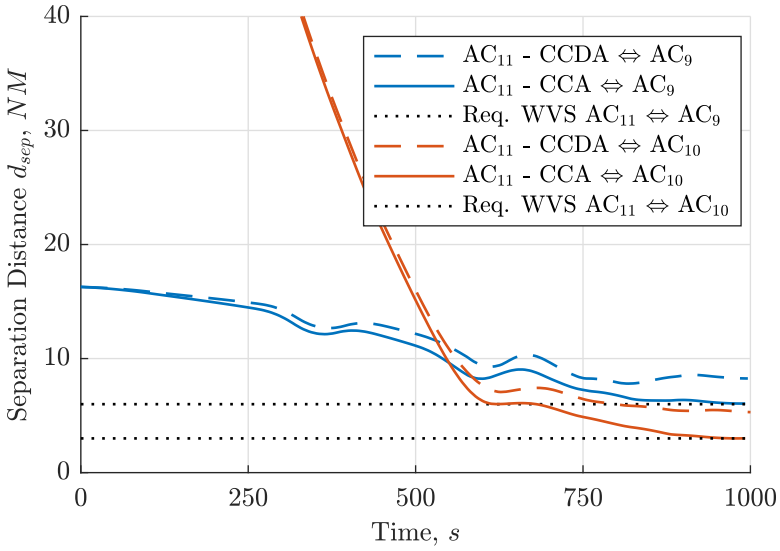

Figure 5.25: Separation distance d_{sep} between AC11 (B733) and AC9 (B738) and, AC11 (B733) and AC10 (B738), with a time difference Δt of 128 *s* and 106 *s* respectively.

Table 5.16: Flight time comparison of all aircraft in scenario 8.

AIRCRAFT NO. & TYPE	DIRECTION	FLIGHT TIME - CCDA (*s*)	FLIGHT TIME - CCA (*s*)	FLIGHT TIME DIFFERENCE WITH CCDA (*s*)
AC1 - B738	South	996.92	996.92	0
AC2 - B744	East	1015.05	1015.29	00.24
AC3 - B744	East	1015.05	1015.05	0
AC4 - MD11	South	996.50	996.50	0
AC5 - B733	East	953.06	1017.97	64.91
AC6 - B733	East	953.06	1002.72	49.66
AC7 - B733	East	953.06	970.33	17.27
AC8 - B738	South	996.92	996.92	0
AC9 - B738	West	996.17	996.17	0
AC10 - B738	South	996.92	1037.31	40.39
AC11 - B733	West	952	992.19	40.9

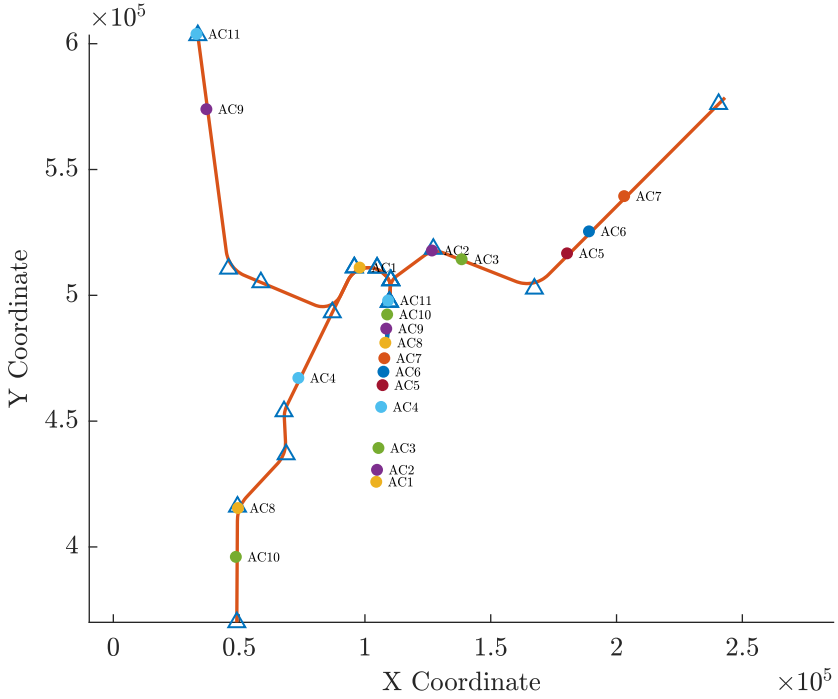

Figure 5.26: Spatial positions of all aircraft at the start and end of optimization of AC11.

The spatial positions of all aircraft before and after optimization of AC11 are depicted in figure 5.26. The large separation between AC3 and AC4 is clearly noticeable in this figure due to the large time difference of 197 *s* between them. It must be noted that unlike in scenario 7 it is possible to optimize more aircraft for a CCA due to the large time differences between the preceeding aircraft pairs.

5.6.3 Scenario 9 - Evening Arrival Peak Period (16:57 - 17:03)

This scenario is meant to highlight the effectiveness of the distance separation algorithm for a highly constrained case. All information pertaining to the aircraft sequence considered in this scenario is shown in table 5.17.

Table 5.17: Aircraft sequence for scenario 9.

AC no.	Actual AC Type	Chosen AC Type	Direction	Sector Entering Time (*hh:mm:ss*)	Time difference with previous AC (*s*)
AC1	F70	B733	South	16:57:12	-
AC2	F70	B733	East	16:57:17	5
AC3	A320	B738	West	16:57:26	9
AC4	F70	B733	West	16:59:02	96
AC5	F100	B733	South	17:00:05	63
AC6	B738	B738	East	17:00:14	9
AC7	F100	B733	East	17:02:43	149
AC8	F70	B733	West	17:02:48	5

Table 5.18: Flight time comparison of all aircraft in scenario 9.

AIRCRAFT NO. & TYPE	DIRECTION	FLIGHT TIME - CCDA (*s*)	FLIGHT TIME - CCA (*s*)	FLIGHT TIME DIFFERENCE WITH CCDA (*s*)
AC1 - B733	South	952.72	952.72	0
AC2 - B733	East	953.06	1005.45	52.39
AC3 - B738	West	996.17	1059.54	63.37
AC4 - B733	West	952	1021.05	69.05
AC5 - B733	South	952.72	1018.50	65.78
AC6 - B738	East	997.67	1066.35	68.68
AC7 - B733	East	953.06	978.32	25.26
AC8 - B733	West	952	1032.30	80.3

It can observed from table 5.17 that the time difference between AC1 - AC2 (Δt of 5 *s*) and AC2 - AC3 (Δt of 9 *s*) results in a highly constrained optimization, similar to scenario 4. Having a large time difference between AC3 - AC4 (Δt of 96 *s*) and AC4 - AC5 (Δt of 63 *s*) is beneficial because, as it can be observed from 5.18, the flight time of CCA of AC4 and AC5 is less than AC3. In other words, AC4 and AC5 are faster than AC3. Hence, due to the large time difference between two consecutive aircraft pairs, AC4 and AC5 do not reduce their CAS and decelerate faster. Although the time difference is less between AC5 - AC6 (Δt of 9 *s*), the large time difference between AC3 - AC4 (Δt of 96 *s*) and AC4 - AC5 (Δt of 63 *s*) helps in optimizing AC6. If the time difference between AC3 - AC4 or AC4 - AC5 pair was also below 10 *s*, the problem might be infeasible for optimization of AC6.

In spite of the large time difference between AC6 - AC7 pair (Δt of 149 *s*), the reduced time difference between AC7 - AC8 (Δt of 5 *s*) pair proves to be a big disadvantage for optimizing AC8. This is because AC8 is not only constrained to maintain minimum WVS separation with AC7, but also with AC6. This implies that AC8 is in conflict with AC7 and AC6, forcing it to reduce it's CAS and decelerate slower than all other aircraft in the sequence, resulting in the largest flight time difference between CCA and CCDA for AC8.

Therefore, if the time difference Δt between any two consecutive aircraft pairs is fairly large or if a trailing aircraft enters the sector after a fairly large duration such that it is not in conflict with the two aircraft that are ahead of it, the last trailing aircraft follows a CCDA or a trajectory closer to a CCDA, making it feasible to optimize further incoming aircraft. If either of the above two conditions are satisfied, a rolling scenario can also be simulated in which one hour of AMS airport's inbound flights are optimized for CDAs.

5.7 AIRCRAFT TRAJECTORY OPTIMIZATION - TIME BASED SEPARATION

The design for aircraft trajectory optimization using TBS is based on the current implementation at the LHR airport. At LHR airport, all aircraft continue to be radar vectored on to the final approach and are only separated based on time during the *final approach* of the aircraft. In order to faciliate this in GPOPS, the problem is formulated in 3 phases. The limits for each of the 3 phases is shown in table 5.19. The TBS is only applied for phase 3 of the problem when the aircraft is on the final approach. In TBS, the optimization is designed to end when the aircraft is at the runway threshold. The other parameters for aircraft trajectory optimization using TBS are shown in table 5.20.

Table 5.19: Initial and terminal phase conditions for Time Based Separation.

PHASE	INITIAL ALTITUDE (ft)	INITIAL SPEED (kts)	FINAL ALTITUDE (ft)	FINAL SPEED (kts)	FINAL DISTANCE (km)
1	30000	303.8 CAS	10000	≤ 250 CAS	-
2	10000	≤ 250 CAS	-	-	172.6
3	-	-	0	160 CAS	d_e

Table 5.20: Optimization parameters for Time Based Separation.

PARAMETER	VALUE
Cost function	Time
Arrival Runway	18R
Lateral Path Waypoints	EEL - ARTIP - NARIX - EH608 - RWY18R
Effective Distance (d_e)	188.89 km
No. of Phases	3
Aircraft Types	B733, B738, B744 & MD11

The conditions defined by the equations 5.1-5.4 are also applicable in this case. The flight path angle γ condition represented by the equation 5.4 is also extended for phase 3.

The leading aircraft AC1 is optimized for the parameters defined in table 5.19 and 5.20. The trailing aircraft AC2 is also optimized for the same initial and final conditions in each phase as the leading aircraft AC1, but with the additional time separation constraint in phase 3. It is applied as a path constraint and is given by the equation,

$$(t_{req} - 1) \leq t_{sep}^{(3)} \leq (t_{req} + 1) \tag{5.18}$$

where t_{req} is the required time separation between the leading and the trailing aircraft along the final approach path. The required time separation t_{req} is defined based on table 5.21, obtained from the NATS aeronautical circular[29]. In cases where the required time separatioin t_{req} between the aircraft is not clearly defined (for example, medium - heavy combination), a minimum of 68 s is assumed. Also, in TBS, the required time separation t_{req} has to be strictly adhered to. Hence, only a small margin of ± 1 s is provided.

Table 5.21: Minimum required time separation t_{req} between two aircraft along the final approach path.

		Trailing		
	WEIGHT CATEGORY	SMALL	MEDIUM	HEAVY
Leading	SMALL	68	68	68
	MEDIUM	90	68	68
	HEAVY	135	113	90

The lateral path chosen for aircraft trajectory optimization using TBS is shown in figure 5.27. It can be observed that the lateral path of the aircraft is extended until the runway threshold,

resulting in more effective distance d_e. The initial altitude of the aircraft is also increased from 28000 *ft* to 30000 *ft* to avoid extended level segments to absorb the excess energy.

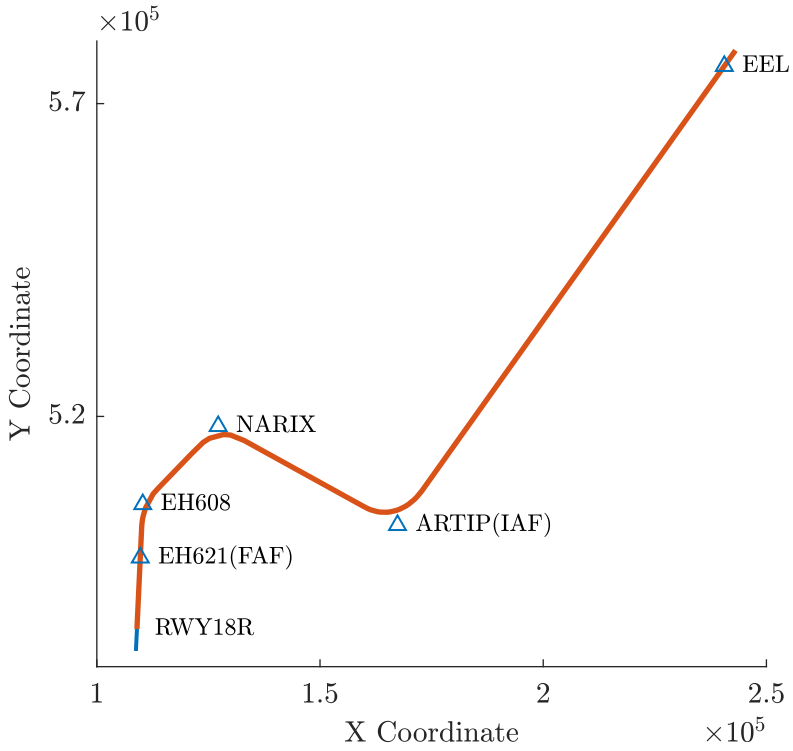

Figure 5.27: Lateral path followed by the aircraft in trajectory optimization using TBS.

The methodology discussed in section 4.4.3 is applied to the following scenarios,

- Scenario 10 - Optimization of a B733 trailing an optimized B738
- Scenario 11 - Optimization of 6 aircraft sequence

5.7.1 Scenario 10 - Optimization of a B733 Trailing an Optimized B738

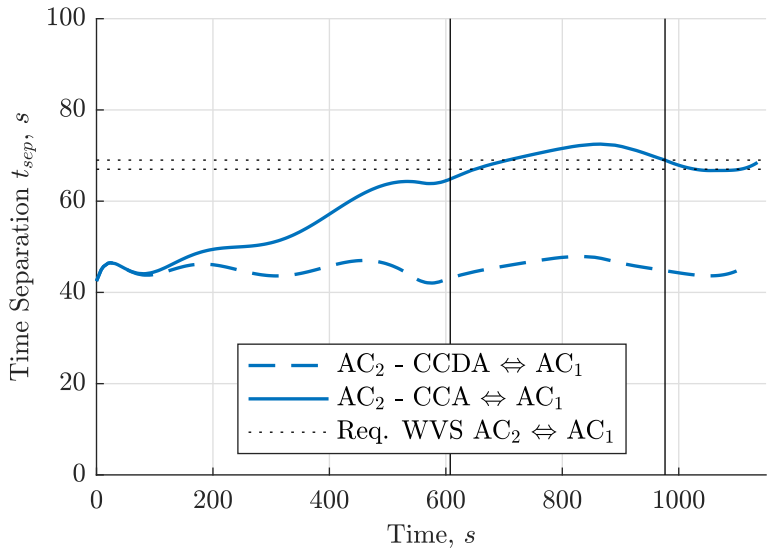

Figure 5.28: Time separation t_{sep} between AC1 (B738) and AC2 (B733) with an initially assumed time lag Δt of 45 *s*.

The leading aircraft AC1 (B738) is optimized for the conditions defined in table 5.19. The trailing aircraft AC2 (B733) enters the sector along the same lateral path - East-18R after an initially assumed time lag Δt, obtained from table 5.5. The variation of time separation t_{sep} between AC1 (B738) and AC2 (B733) with respect to the flight time is shown in figure 5.28. The end of phase 1 and end of phase 2 are also marked in this figure for reference. It can be observed that the optimizer successfully manages to separate the two aircraft in phase 3, within the limits defined by equation 5.18. The altitude and CAS profiles of both aircraft are shown in 5.29. In order to ensure sufficient time separation t_{sep}, the CAS of the trailing aircraft AC2 (B733) above 10000 ft is reduced.

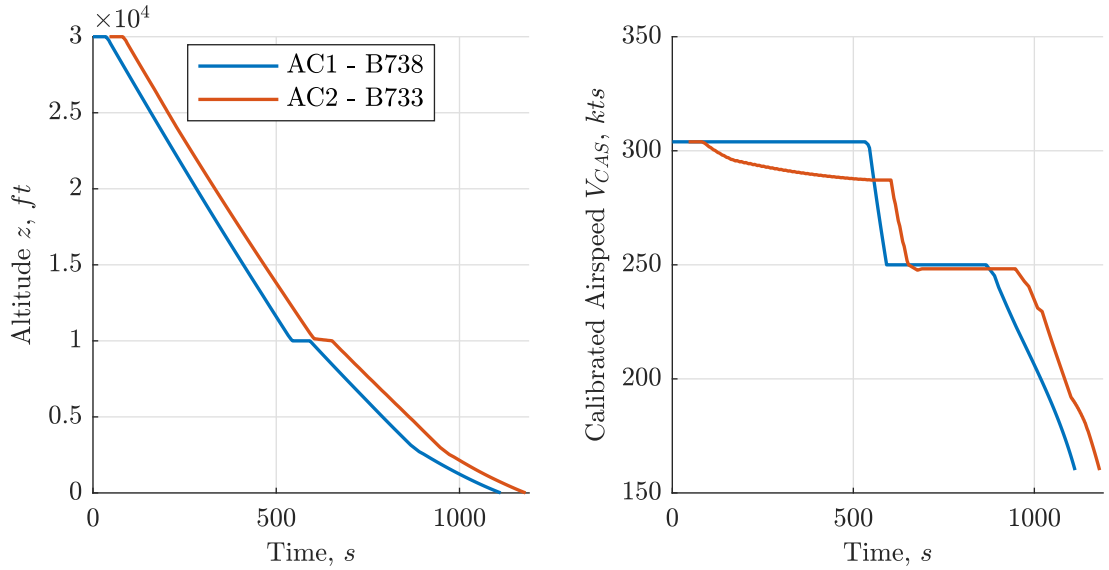

Figure 5.29: Optimization of a B733 trailing an optimized B738 plotted with the initially assumed time lag Δt of 45 *s*. (a) Altitude profile, (b) Calibrated Air Speed profile.

Having a faster aircraft such as the B733 is advantageous in situations where the initially assumed time lag Δt is large. In this scenario if an initially assumed time lag Δt of 120 *s* is considered, the optimizer manages to separate the two aircraft with the required time separation t_{sep} of 68 ± 1 *s*.

Optimization of a B733-B744 aircraft pair, with an initially assumed time lag Δt of 45 *s* results in infeasibility. This is because the trailing aircraft AC2 (B744) is slower than the leading aircraft AC1(B733) by approximately 80 *s*. This in turn results in large time separation between the two aircraft and it is not possible to achieve the desired time separation t_{sep} of 56 *s*. The same also holds true for a B733-B738 and a B733-MD11 aircraft pair.

Table 5.22: Aircraft sequence for scenario 11.

AIRCRAFT NUMBER	AIRCRAFT TYPE	TIME DIFFERENCE WITH PREVIOUS AC *(s)*
AC1	B744	-
AC2	B733	180
AC3	B733	40
AC4	B738	35
AC5	MD11	45
AC6	B733	167

5.7.2 Scenario 11 - Optimization of 6 Aircraft Sequence

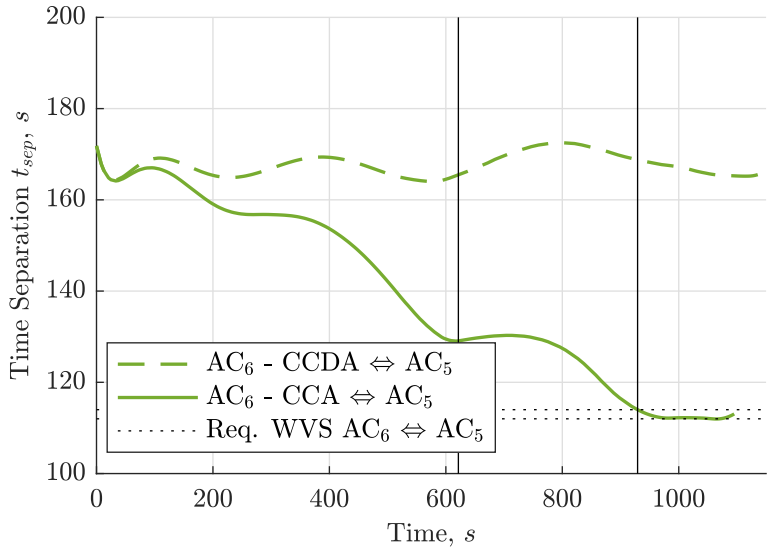

Figure 5.30: Time separation t_{sep} between AC5 (MD11) and AC6 (B733) with an initially assumed time lag Δt of 167 *s*.

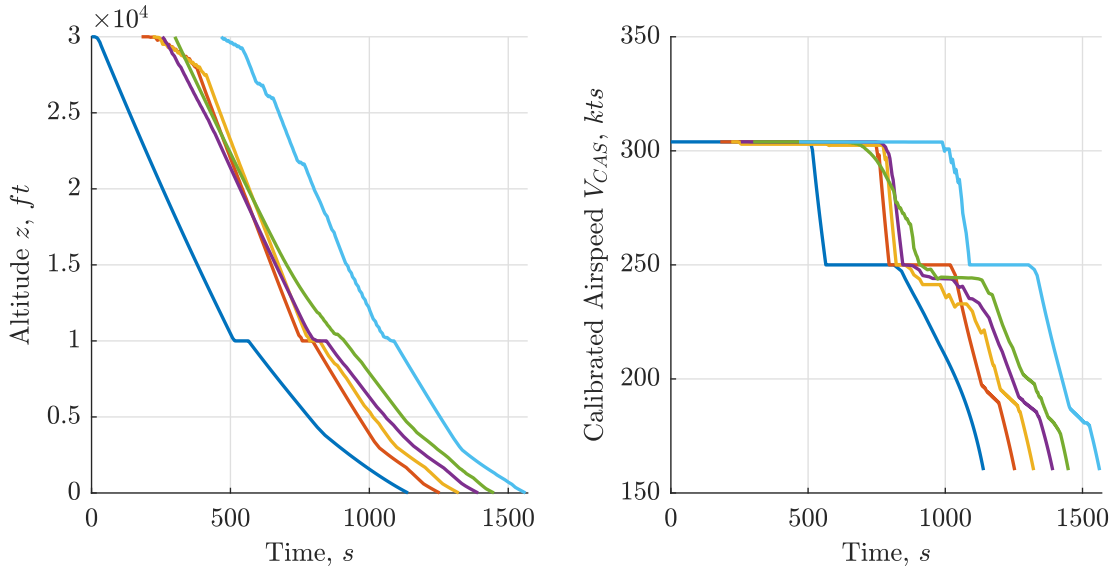

(a) **(b)**

Figure 5.31: Optimized trajectories of all aircraft plotted with the initially assumed time lag Δt. (a) Altitude profile, (b) Calibrated Air Speed profile.

In multi-aircraft trajectory optimization using TBS, the aircraft currently being optimized is required to maintain time separation with only one aircraft ahead of it.

In this scenario, upto 6 aircraft are considered. All the information pertaining to the aircraft sequence considered in this scenario is detailed in table 5.22. The time difference is chosen at random, but by also being aware of the infeasibilities that might occur with certain aircraft pairs and the initially assumed time lag Δt. The variation of the time separation t_{sep} between AC5 and AC6 with respect to flight time is shown in figure 5.30. It can be observed that due to the B733 aircraft being faster than a MD11 aircraft, the time separation between them is reduced from 167 *s* to the required 113 *s*. The altitude and CAS profiles of all six aircraft are shown in figure 5.31.

The figures clearly highlight the mainatined time separation between each aircraft pair at the terminal point.

5.8 Comparison of Computation Times

When attempting to optimize the trajectorties of aircraft in real-time by the ATC, the computation time required by GPOPS to arrive at an optimal solution is of paramount importance. This section is intended to provide an estimate of the computation time required to arrive at the optimal solution for certain scenarios considered in this chapter. It is important to note here that the computation time is the time required to optimize all aircraft in a scenario and not just the computation time required to optimize the last trailing aircraft. The approximate computation time taken by GPOPS to arrive at an optimal solution is shown in table 5.23 for selected scenarios.

Table 5.23: Comparison of computation time for selected scenarios.

Scenario	Number of AC	Computation time *(s)*
Single aircraft	1	7
SC 1	2	10
SC 2	2	10
SC 3	2	8
SC 4	2	36
SC 5	2	12
SC 6	10	341
Fuel vs Time (Fuel)	5	62
Fuel vs Time (Time)	5	190

All the simulations using GPOPS were performed on a computer which was equipped with an Intel 6^{th} generation 2.9 *GHz* dual-core i5 processor coupled with 8 *GB* of RAM. The computing power of the processor has an influence on the computation time of all simulated scenarios. Single-aircraft trajectory optimization takes less than 10 *s* with a new guess. It can be observed from table 5.23 that scenario 1 and scenario 2 computation time are shorter due to the problem being less constrained. Scenario 3 computation time is similar to single aircraft due to the redundant separation distance constraint. Computation time for aircraft trajectory optimization along different lateral paths is longer than for aircraft trajectory optimization along the same lateral path due to the additional computation related to computing the spatial positions of all aircraft and re-converting it to distance at all the nodes.

In a highly constrained problem and when more than 4-5 aircraft are being optimized, if the initial guess is not the same as that of the aircraft type being currently optimized, the computation time can be very large - up to 6 minutes, in rare cases up to 20-25 minutes; but if the initial guess is similar to the aircraft type being currently optimized, the computation time can be much shorter (less than 2 minutes). Hence, in certain situations, it is beneficial from a computation time point of view to initiate the initial guess of the same aircraft type. SNOPT also has an influence on the computation time and it's effect is highly unpredictable. Sometimes, even for a less constrained problem, converging to an optimal solution requires multiple iterations, but sometimes it can arrive at an optimal solution for the same set of conditions with very less number of iterations.

6

Conclusions and Recommendations

The current thesis focused on overcoming some of the limitations pertaining to the widespread implementation of Continuous Descent Arrivals, with the help of optimal control theory. The focus was to successfully maintain the required time or distance separation between aircraft, while still being able to perform as close as possible to a CDA. Using optimal control theory, either fuel or time optimized aircraft trajectories are obtained. It helps in overcoming one of the major limitations of CDAs - trajectory unpredictability. The optimization is carried out by the ATC and the trajectory is uplinked to the aircraft, with the help of ADS-B. The flight crew can then input the optimized trajectory into the FMS of the aircraft before it reaches TOD and follow it. If all aircraft follow the optimal trajectories, the ATC can always be aware of the spatial position of every aircraft in the sector. Since the optimal trajectories of aircraft already ensure sufficient separation between aircraft, the ATC will no longer have to enforce more separation between them. This will, in turn, facilitate the use of CDAs in medium-high density traffic conditions at airports around the world.

6.1 Conclusions

The aircraft separation algorithm when coupled with GPOPS has been successfully used to ensure that all aircraft can maintain sufficient separation along the entire trajectory of the aircraft. The main objective of the thesis to use optimal control theory to enable multi-aircraft trajectory optimization for CDAs while ensuring sufficient separation between them has been achieved.

Aircraft trajectory optimization along the same lateral path (SC1-SC3), as well as different lateral paths (SC4-SC6), but merging at a common waypoint before landing on a single runway has been studied in detail. The effect of the initially assumed time lag and the fleet mix and on the on the separation algorithm, the flight time, the delay and penalty incurred by the trailing aircraft is demonstrated.

Although the focus of the thesis is to obtain time optimized trajectories, a comparison is done between fuel and time optimized trajectories. The flight time and the fuel consumed, along with the differences in the obtained trajectories and shortcomings of fuel optimized trajectories are discussed in detail. Time optimized trajectories offer a clear advantage when a large sequence of aircraft are to be optimized for CDA.

It was simulated using AMS airport's real-time inbound flight data that during the arrival peak hours and non-peak hours, it is possible to optimize all the aircraft coming from different directions for CDAs and land on a single runway (SC7-SC9). The AMS airport real-time inbound flight data clearly demonstarted the robustness of the optimizer. In order to optimize more than 10 - 11 aircraft, it is beneficial to have sufficiently large time difference between any two consecutive aircraft pairs or very large time difference such that the last trailing aircraft is not in conflict with the two aircraft ahead of it. This ensures that the last trailing aircraft follows a CCDA without any separation constraint violation, making it easier to optimize further incoming aircraft.

Since the lateral path designs used in this thesis are based on RNAV night arrivals at the AMS airport, the aircraft are already being flown on less populated areas and the noise generated by them is concentrated along the pre-defined lateral paths only. Fixing the descent trajectories of all the leading aircraft to optimize the descent trajectory of the trailing aircraft is benefical in keeping the computation time in check (due to less constraints), but disadvantageous for the trailing aircraft which incurs all the penalty. The penalty is always in the form of velocity reduction, since no path extension or path shortening techniques are implemented in the design of the algorithm except for scenario 5. It was demonstrated that it is possible for a faster trailing aircraft to land ahead of the slower leading aircraft by employing path shortening and inducing a penalty on the objective function.

The possibility of using TBS for aircraft trajectory optimization is shown in this thesis. Although it will take up to a decade before the current ICAO's Distance Based Separation is completely replaced with Time Based Separation, airport's around the world are beginning to implement TBS on final approaches to increase the runway throughput in heavy to light headwind conditions. The results of aircraft trajectory optimization using TBS show that it is indeed possible to separate multiple aircraft on final approach by separating them within specific time limits. The bounds for TBS are different and much more stringent. This in turn results in some limitations; certain aircraft pairs cannot be optimized.

The simulation design used for this thesis is based on the geography of the AMS airport. It is important to note that the methodology can be used for any airport around the world. The only difference would be that lateral paths to be followed by the aircraft will have to be designed specific for that airport. Hence, the separation algorithm is generic and can be used for any airport around the world.

6.2 Recommendations and Future Work

The availability of limited aircraft models lead to some assumptions in the simulation using AMS airport's real-time inbound flight data. Also, the actual altitude and the speed of each aircraft is discounted for the purpose of simulations. The aircraft type has a significant impact on the results due to individual aircraft performance characteristics. It would be interesting to perform the simulations with more diverse aircraft types, employ path stretching or path shortening techniques, using the actual speed and the altitude of each aircraft and study the influence on the results.

Although the simulations in this thesis are based on the advanced CDA technique, tactical CDA can have certain advantages. In a tactical CDA, aircraft can be vectored onto the final approach. In addition to the existing pre-defined lateral paths, shorter paths can be designed between the same initial and final waypoints. This would facilitate a faster trailing aircraft entering the sector after a short time interval Δt to reach the terminal point before the leading aircraft by following the shorter path, but with a penalty on the objective function. It will also be beneficial for the whole simulation environment, since some trailing aircraft will not have to decelerate slowly

and reduce their CAS, in turn, allowing more aircraft to be optimized.

In an effort to make the simulation environment depict a real-time operating environment, simultaneous arrivals on two runways can be simulated. Such a scenario, coupled with additional lateral paths will provide significant benefits in improving the capabilities of the simulation environment and overcome the major shortcoming of DBS. With the use of an additional runway, runway throughput can be increased. Secondly, the whole aircraft sequence in consideration becomes much less constrained, leading to faster computation times, reduces the penalty incurred by the trailing aircraft to maintain the required separation and allows more aircraft to be optimized.

A lot of assumptions are made during the implementation of the model in GPOPS. Firstly, the effect of winds are not considered in the aircraft performance models or in the design of the separation algoritm, although, TBS addresses the effect of headwinds on final approach. The effect of winds at the AMS airport are predominant throughout the year. It would be interesting to study the effect of wind on the separation algorithm and the simulation results.

More improvements can be made to address some of the shortcomings of the TBS. An attempt can be made to reduce the margin of ± 1 s over the required time separation. The resulting time separation between aircraft will be more precise and accurate. TBS can also be extended to be implemented on aircraft approaching from different lateral paths, similar to what is demonstrated in DBS. In a real-time operating evnironment it is not possible for the controller to choose the time difference Δt between the aircraft when attempting to separate aircraft using TBS. Hence, a combination of both DBS and TBS can be used. In high desnsity traffic conditions, the aircraft can be separated on final approach using TBS, whilst following a CDA. In low-medium density traffic conditions, aircraft can be separated using the conventional DBS, whilst following a CDA.

At this point, it is clear that although the research objective of this thesis has been answered, it is far from ideal to be used in a real-time operating evnvironmen. Future work and the recommendations can significantly improve the simulation environment. A lot of practical limitations would still need to be addressed. Firstly, a ground based automation tool is required to allow ground controllers to compute the optimal trajectories and uplink it to the aircraft. Secondly, the FMS of all aircraft must be capable of following the optimal trajectories uplinked to the aircraft. Finally, it would be beneficial if each aircraft can communicate it's spatial position to other aircraft and facilitate revision of the optimal trajectories in real-time, with minimal involvement from the ATC, in the event of a collision. Nevertheless, the implementation of the separation algorithm to manage the separation of all aircraft whilst following a trajectory as close as possible to CDAs, brings us a little closer in realising the wide-spread implementation of CDAs in medium-high density traffic conditions. Futher improvements to the simulation environment will allow us to bridge the gap between a real-time operating environment and a simulation environment. With sufficient improvements to the current technologies, in the near future it might be possible to perform trial runs and validate the results obtained from the simulations.

BIBLIOGRAPHY

[1] BERNELLI-ZAZZERA, F., VASILE, M., FORNASARI, N., AND MASARATI, P. Design of Interplanetary and Lunar Missions Combining Low Thrust and Gravity Assists. *Final Report of ESA/...*, 14126 (2002), 76.

[2] BETTS, J. T. Survey of Numerical Methods for Trajectory Optimization. *Journal of Guidance, Control, and Dynamics 21*, 2 (1998), 193–207.

[3] BETTS, J. T., AND HUFFMAN, W. P. Sparse optimal control software SOCS. *Mathematics and Engineering Analysis Technical Document MEA-LR-085, Boeing Information and Support Services, The Boeing Company, PO Box 3707*, 92207–98124.

[4] CAGE, P., KROO, I., AND BRAUN, R. Interplanetary trajectory optimization using a genetic algorithm. In *Astrodynamics Conference*, Guidance, Navigation, and Control and Co-located Conferences. American Institute of Aeronautics and Astronautics, aug 1994.

[5] CLARKE, J.-P., HO, N. T., REN, L., BROWN, J. A., ELMER, K. R., ZOU, K., HUNTING, C., MCGREGOR, D. L., SHIVASHANKARA, B. N., TONG, K.-O., WARREN, A. W., AND WAT, J. K. Continuous Descent Approach: Design and Flight Test for Louisville International Airport. *Journal of Aircraft 41*, 5 (2004), 1054–1066.

[6] DARBY, C. L., HAGER, W. W., AND RAO, A. V. An hp-adaptive pseudospectral method for solving optimal control problems. *Optimal Control Applications and Methods 32*, 4 (2011), 476–502.

[7] DE JONG, P. M. A., DE GELDER, N., VERHOEVEN, R., BUSSINK, F. J. L., KOHRS, R., VAN PAASSEN, M. M., AND MULDER, M. Time and Energy Management During Descent and Approach: Batch Simulation Study. *Journal of Aircraft 52*, 1 (2014), 1–14.

[8] EUROCONTROL. Continuous Descent Approach - Implementation Guidance Information. Tech. rep., 2008.

[9] EUROCONTROL. Environmental issues for aviation [Accessed on 10 June 2016] URL: http:// www. eurocontrol. int/ articles/ environmental-issues-aviation, 2016.

[10] FEDERAL AVIATION ADMINISTRATION (FAA). Aeronautical Information Manual. Tech. rep., FAA, 2014.

[11] GARG, D., PATTERSON, M., HAGER, W. W., RAO, A. V., BENSON, D. A., AND HUNTINGTON, G. T. A unified framework for the numerical solution of optimal control problems using pseudospectral methods. *Automatica 46*, 11 (2010), 1843–1851.

[12] GATH, P., AND WELL, K. Trajectory optimization using a combination of direct multiple shooting and collocation. In *AIAA Guidance, Navigation, and Control Conference and Exhibit*, Guidance, Navigation, and Control and Co-located Conferences. American Institute of Aeronautics and Astronautics, aug 2001.

[13] GELFAND, I., AND FOMIN, S. *Calculus of Variations*, 2000 ed. Dover Publications, Mineola, New York.

[14] GILL, P. E., MURRAY, W., AND SAUNDERS, M. A. SNOPT: An SQP Algorithm for Large-Scale Constrained Optimization. *SIAM Journal on Optimization 12*, 4 (2002), 979–1006.

[15] HANS JOACHIM OBERLE, AND GRIMM, W. BNDSCO - A program for the Numerical Solution of optimal Control Problems, 1989.

[16] HARALDSDOTTIR, A., SCHARL, J., BERGE, M. E., SCHOEMIG, E. G., AND COATS, M. L. Arrival Management with Required Navigation Performance and 3D Paths. *USA/Europe Air Traffic Management Research and Development Seminar* (2007), 1–12.

[17] HARGRAVES, C., AND PARIS, S. Direct trajectory optimization using nonlinear programming and collocation. *Journal of Guidance, Control, and Dynamics 10*, 4 (jul 1987), 338–342.

[18] HARTJES, S. *An Optimal Control Approach to Helicopter Noise and Emissions Abatement Terminal Procedures*. Uitgeverij BOXPress, 's-Hertogenbosch, 2015.

[19] HUNTINGTON, G. Advancement and analysis of a Gauss pseudospectral transcription for optimal control problems. 207.

[20] IATA. A global approach to reducing aviation emissions. First stop : carbon-neutral growth by 2020. Tech. rep., 2009.

[21] IATA. IATA Welcomes New CO2 Emissions Standard for Aircraft [Accessed on 07 October 2016] URL : http://www.iata.org/pressroom/pr/Pages/2016-02-09-01.aspx, 2016.

[22] INTERNATIONAL CIVIL AVIATION ORGANIZATION (ICAO). Review of noise abatement procedure research & development and implementation results.

[23] KERSHAW, A. The influence of ATC in approach noise abatement. *3rd USA/Europe Air Traffic ...*, June (2000), 13–16.

[24] KLOOSTER, J. K., WICHMAN, K. D., AND BLEEKER, O. F. 4D Trajectory and Time-of-Arrival Control to Enable Continuous Descent Arrivals. *AIAA Guidance, Navigation, and Control Conference*, August (2008), 1–17.

[25] LIMEBEER, D. J. N., AND RAO, A. V. Faster, Higher, and Greener: Vehicular Optimal Control. *IEEE Control Systems 35*, 2 (2015), 36–56.

[26] LU, P., SUN, H., AND TSAI, B. Closed-Loop Endoatmospheric Ascent Guidance. *Journal of Guidance, Control, and Dynamics 26*, 2 (2003), 283–294.

[27] LUCHTVERKEERSLEIDING NEDERLAND (LVNL). Baangebruik Schiphol [Accessed on : 24-10-2016] URL: http://www.lvnl.nl/omgeving/baangebruik.html.

[28] MEIJER, L. K., DE GELDER, N., MULDER, M., VAN PAASSEN, M. M., AND IN 'T VELD, A. C. Time-based Spaced Continuous Descent Approaches in busy Terminal Manoeuvring Areas. *AIAA Guidance, Navigation, and Control*, August (2009), 1–23.

[29] NATIONAL AIR TRAFFIC SERVICES. Aeronautical Information Circular P 3 / 2014. 1–12.

[30] PARK, S. G., AND CLARKE, J.-P. Feasible Time Range Analysis of Wide Fleet for Continuous Descent Arrival. *2013 Aviation Technology, Integration, and Operations Conference*, August (2013), 1–15.

[31] PARK, S. G., AND CLARKE, J.-P. Trajectory Generation for Optimized Profile Descent using Hybrid Optimal Control. *Guidance, Navigation, and Control and Co-located Conferences* (2013), 1–14.

[32] PARK, S. G., AND CLARKE, J.-P. Optimal Control Based Vertical Trajectory Determination for Continuous Descent Arrival Procedures. *Journal of Aircraft 52*, 5 (2015), 1469–1480.

[33] PARK, S. G., CLARKE, J.-P., FERON, E., AND JIMENEZ, H. Encounter Rate Estimation of Continuous Descent Arrival Procedures in Terminal Area. *AIAA Guidance, Navigation, and Control Conference*, January (2016), 1–14.

[34] PRATS, X., PÉREZ-BATLLE, M., BARRADO, C., VILARDAGA, S., BAS, I., BIRLING, F., VERHOEVEN, R. P. M., AND MARSMAN, A. Enhancement of a time and energy management algorithm for continuous descent operations. *14th AIAA Aviation Technology, Integration, and Operations Conference, AIAA Aviation and Aeronautics Forum and Exposition 2014*, June (2014), 1–11.

[35] RAO, A. V. A survey of numerical methods for optimal control. *Advances in the Astronautical Sciences 135*, 1 (2009), 497–528.

[36] RAO, A. V., BENSON, D. A., DARBY, C., PATTERSON, M. A., FRANCOLIN, C., SANDERS, I., AND HUNTINGTON, G. T. Algorithm 902: GPOPS, A MATLAB Software for Solving Multiple-Phase Optimal Control Problems Using the Gauss Pseudospectral Method. *ACM Transactions on Mathematical Software 37*, 2 (2010), 1–39.

[37] ROSS, I. M., SEKHAVAT, P., FLEMING, A., AND GONG, Q. Pseudospectral Feedback Control: Foundations, Examples and Experimental Results. *Proceedings of the AIAA Guidance, Navigation, and Control Conference and Exhibit*, August (2006), 1–23.

[38] TONG, K.-O., BOYLE, D. A., AND WARREN, A. W. Development of Continuous Descent Arrival (CDA) Procedures for Dual-Runway Operations at Houston Intercontinental. *Design*, September (2006), 25–27.

[39] TONG, K. O., SCHOEMIG, E. G., BOYLE, D. A., SCHARL, J., AND HARALDSDOTTIR, A. Descent profile options for continuous descent arrival procedures within 3D path concept. *AIAA/IEEE Digital Avionics Systems Conference - Proceedings* (2007), 1–11.

[40] VISSER, H. G., AND WIJNEN, R. A. A. Optimization of Noise Abatement Arrival Trajectories. *Journal of Aircraft 38*, 4 (2001), 620–627.

[41] VON STRYK, O. Userguide for DIRCOL: A direct collocation method for the numerical solution of optimal control problems. *Lehrstuhl für Höhere Mathematik und Numerische*, November (1999).

[42] WAT, J., FOLLET, J., MEAD, R., BROWN, J., KOK, R., DIJKSTRA, F., AND VERMEIJ, J. In Service Demonstration of Advanced Arrival Techniques at Schiphol Airport. *AIAA*, September (2006), 25 – 27.

[43] WUBBEN, F. J. M., AND BUSINK, J. J. Environmental Benefits of Continuous Descent Approaches At Schiphol Airport Compared With Conventional Approach Procedures. 1–5.